arXiv:1703.09598v1 [physics.flu-dyn] 28 Mar 2017

Caustic conditions for d-dimensional Lagrangian fluids

Job Feldbrugge[1]†, Rien van de Weygaert[2], Johan Hidding[2] and Joost Feldbrugge[3]

[1]Perimeter Institute for Theoretical Physics, University of Waterloo, Waterloo, Canada
[2]Kapteyn Astronomical Institute, University of Groningen, The Netherlands
[3]JFA Feldbrugge Studios, Lettelbert, The Netherlands

(Received xx; revised xx; accepted xx)

Caustics form in Lagrangian fluids when fluid elements cross and multi-stream regions form. For low-dimensional Lagrangian fluids, the caustics have been classified by catastrophe theory. In the case of potential flow, for one- and two-dimensional fluids, Arnol'd *et al.* (1982) related this classification to conditions on the displacement field of the fluid. These conditions are called the *caustic conditions*. This paper concerns nothing less than an entirely new proof for the classification of Lagrangian catastrophes. We provide an alternative, more direct and transparent, path towards the classification of singularities as proposed by Arnol'd. In this study we give a novel derivation of the caustic conditions for the explicit situation of three-dimensional fluids, following up on those for one- and two-dimensional fluids. Moreover, our derivation scheme allows us to extend these to general Lagrangian fluids in spaces of arbitrary dimensions. Applications to cosmic structure formation and to turbulence are indicated, and shortly discussed. In an accompanying publication we apply this towards a full three-dimensional study of caustics in the context of the formation of the cosmic web.

Key words: Mathematical foundations, General fluid mechanics, Shock waves, Compressible flows, Large-scale structure formation

1. Introduction

Caustics are important features in the dynamics of fluids, marking the positions where fluid elements cross and multi-stream regions form. The caustics can be associated to the regions with infinite Lagrangian density, nearly always corresponding to locations where shell-crossing occurs or where we see the formation of shocks. In the context of the formation of cosmic structure, caustics mark the regions where non-linear gravitational collapse starts to take place and the cosmic web begins to form (Zel'dovich 1970; Bond *et al.* 1996; van de Weygaert & Bond 2008; Cautun *et al.* 2014).

Caustics in Lagrangian fluids with Hamiltonian dynamics are classified by Lagrangian catastrophe theory (Arnol'd 1976, 1982). Soon after Arnol'ds work, these results were extended to generic Lagrangian fluid dynamics (Bruce 1985). For the classification of caustics emerging in the context of a one- and two-dimensional description of cosmic structure formation by the Zel'dovich approximation, Arnol'd *et al.* (1982) translated

† Email address for correspondence: jfeldbrugge@perimeterinstitute.ca

this into conditions on the displacement field. Following up on this seminal work, in a more recent study Hidding *et al.* (2014) analyzed the overall morphology and connectivity of caustics that emerge in a displacement field described by the one- and two-dimensional Zel'dovich approximation. The visual illustration of the emerging structure, for a field of initially Gaussian random density and potential fluctuations, revealed how the caustics spatially outline the spine of the cosmic web. Feldbrugge *et al.* (2014) elaborated this into an analytical evaluation of the statistical properties of caustics, assuming an random Gaussian initial density and potential field.

In the current study, we give a novel proof of the caustic conditions for the explicit situation of three-dimensional fluids, following up on those for one- and two-dimensional fluids. It provides an alternative, more direct and transparent, path towards the classification of singularities as proposed by Arnol'd (Arnol'd 1976, 1982). Our derivation is an entirely new proof for the classification of Lagrangian catastrophes. Moreover, our scheme allows us to extend these to general Lagrangian fluids in a space of arbitrary dimension. Its generic nature facilitates the derivation of generic caustic conditions, even for a fluid with arbitrary dynamics.

Traditionally the classification of Lagrangian catastrophes was proven algebraically by means of the general formalism of catastrophe theory. The purely geometric proof presented here, based on the geometric description of shell-crossing conditions in combination with Morse-Smale theory (Morse 1934; Milnor 1963), does not rely on this framework of general catastrophy theory. In this, it does not need the use of algebraic topology in terms of jet-spaces, Jacobi ideals and generating functions for Lagrangian map germs. It provides an alternative to Arnol'ds proof for the classification of degenerate critical points. Its importance lies in the fact that it does not invoke such advanced mathematical concepts. Moreover, given the fact that it concerns a more direct and constructive proof, it facilitates its practical application to a range of physical phenomena for the specific situation of Lagrangian fluids.

One specific configuration whose analysis is enabled by our formalism is that of the formation of the cosmic web in the distribution of matter on Megaparsec scales. This will be the subject of the accompanying paper (Feldbrugge *et al.* 2017). It addresses the application of the caustic conditions and the caustic skeleton to the formation of the cosmic web in a fully three-dimensional configuration. The aim is to improve our understanding of the formation of the cosmic web and to attempt the analytical derivation of quantitative properties of the current large-scale structure.

The plan for the present paper starts with section 2, in which we give a concise description of Lagrangian fluid dynamics. The formation of caustics and derivation of the shell-crossing conditions is studied in section 3. These conditions are among the main results presented here. In section 4 we apply these shell-crossing conditions to the classification of catastrophes, described in section 5, to derive the caustic conditions. Finally, in section 6 we describe the dynamical framework resulting from the considerations above.

2. Lagrangian fluid dynamics

There exist multiple approaches to fluid dynamics. In the Eulerian approach, the evolution of the smoothed density and velocity fields is analyzed. The equations of motion of Eulerian fluids are relatively concise and give a reasonably accurate description of the mean flow in a fluid element at a given location in the fluid.

One serious disadvantage of the Eulerian framework is that it does not directly relate to the motion of the particles in the fluid. Because it basically restricts itself to the mean motion in a fluid element, it does not facilitate an accurate description of the evolution

of multi-stream regions. More suited for following the complex dynamical evolution of fluid elements, including the emergence of caustics, is the Lagrangiam approach to fluid dynamics.

In Lagrangian fluid dynamics, we assume every point in space to consist of a mass element. These mass elements flow with the fluid. Their motion is described by a map $x_t : L \to E$, mapping the initial position q in the Lagrangian manifold L to the position $x_t(q)$ of the mass element in the Eulerian manifold E at time t. In the context of Lagrangian fluid dynamics, it is most convenient to describe the evolving fluid in terms of the displacement map $s_t : L \to E$,

$$s_t(q) = x_t(q) - q\,, \tag{2.1}$$

for all $q \in L$. It is important to always assume that the maps x_t and s_t are continuous and sufficiently differentiable. While in the Lagrangian description a mass element has a constant mass, it may contract, expand, deform and even rotate. This is described in terms of the deformation tensor $\mathcal{M}$, the gradient of the displacement field with respect to the Lagrangian coordinates of a mass element,

$$\mathcal{M} \;=\; \frac{\partial s_t}{\partial q} \;=\; \begin{pmatrix} M_{1,1} & M_{2,1} & M_{3,1} \\ M_{1,2} & M_{2,2} & M_{3,2} \\ M_{1,3} & M_{2,3} & M_{3,3} \end{pmatrix}. \tag{2.2}$$

While mass elements in a Lagrangian fluid are characterized by a few fundamental quantities, which characterize them and remain constant throughout their evolution, most physical properties are basically derived quantities. A good example and illustration of a derived quantity is the value of the density in a density field. The density in a point $x' \in E$ is defined as the initial mass in the mass element times the ratio of the initial and final volume of the mass element. Formally, this is expressed as a change of coordinates involving the Jacobian of the map x_t,

$$\begin{aligned} \rho(x',t) &= \sum_{q\in A_t(x')} \rho_i(q) \left|\frac{\partial x_t(q)}{\partial q}\right|^{-1} \\ &= \sum_{q\in A_t(x')} \rho_i(q) \left|1 + \frac{\partial s_t(q)}{\partial q}\right|^{-1} \\ &= \sum_{q\in A_t(x')} \frac{\rho_i(q)}{(1+\mu_{t1}(q))(1+\mu_{t2}(q))(1+\mu_{t3}(q))}, \end{aligned} \tag{2.3}$$

with ρ_i the initial density field and μ_{ti} the eigenvalue fields of the deformation tensor $\mathcal{M}(q)$ (eqn. 2.2). The points $A_t(x')$ are the points q in Lagrangian space L which map to x', i.e., $A_t(x') = \{q \in L | x_t(q) = x'\}$. By substituting derived quantities like density in the, often more familiar, Eulerian fluid equations, we may obtain a closed set of differential equations for the Eulerian position map x or the displacement map s.

Equation 2.3 applies to a fluid with three spatial dimensions. The arguments presented in this paper straightforwardly generalize to a Lagrangian fluid with an arbitrary number of spatial dimension. For simplicity, we will restrict explicit expressions the 3-dimensional

case †. It is straightforward to generalize equation 2.3 to d-dimensional fluids in d-dimensional space.

Of key importance is the implication of equation 2.3 that an infinite Lagrangian density occurs when a mass element is turned inside out. More formally stated, as we will see in section 3, an infinite density occurs when for at least one of the $i = 1, \ldots, d$,

$$1 + \mu_i = 0\,. \tag{2.4}$$

The regions, in which the mapping x_t becomes degenerate and the density becomes infinite are known as *foldings*, *caustics* or *shocks*. They mark important features in the Lagrangian fluid and are the object of study in this paper. Note that for practical reasons in this paper we will sometimes suppress the time index of the eigenvalue fields, i.e. $\mu_i = \mu_{ti}$.

Throughout our study, we assume that the displacement map s_t is continuous and sufficiently differentiable. The corresponding eigenvalues are the roots of the characteristic polynomial of the matrix $\mathcal{M} = \partial s_t/\partial q$. Since the characteristic equation is a non-linear equation, in principle the eigenvalues could develop singularities and become non-differentiable. However, it can be shown that the eigenvalues can be ordered such that they are continuous. Furthermore the eigenvalues will be differentiable whenever the eigenvalues are distinct. When two eigenvalues coincide, the eigenvalue fields may become non-differentiable.

2.1. *Hamiltonian Fluid Dynamics*

In the case of Hamiltonian fluid dynamics, we apply the Hamiltonian formalism to fluid mechanics. This is possible for non-dissipative fluids. To this end, the mass density field ρ and the velocity potential ϕ,

$$v = \nabla\phi \tag{2.5}$$

function as conjugate fields. The resulting two equations of motion then read as

$$\begin{aligned} \frac{\partial\rho}{\partial t} &= +\frac{\partial\mathcal{H}}{\partial\phi} = -\nabla\cdot(\rho v)\,, \\ \frac{\partial\phi}{\partial t} &= -\frac{\partial\mathcal{H}}{\partial\rho}\,, \end{aligned} \tag{2.6}$$

with the Hamiltonian $\mathcal{H}$ defined by the integral expression

$$\mathcal{H} = \int \mathrm{d}x \left(\frac{1}{2}\rho(\nabla\phi)^2 + e(\rho)\right)\,, \tag{2.7}$$

where $e(\rho)$ is the internal energy as a function of density ρ. The first equation of motion in equation 2.6 is equivalent to the continuity equation, while the second equation implies the Euler equation

$$\frac{\partial v}{\partial t} + v\cdot\nabla v = -\frac{1}{\rho}\nabla p\,, \tag{2.8}$$

in which p is the pressure of the fluid. For a thorough discussion of Hamiltonian mechanics and Hamiltonian fluids we refer to the seminal volumes of Goldstein (1980), Landau & Lifshitz (1976), Landau & Lifshitz (1959) and Arnol'd (1978).

† Formally, it would be appropriate to describe the fluids as $(d+1)$-dimensional fluids, a combination of their embedding in a d-dimensional space along with their evolution along time dimension t.

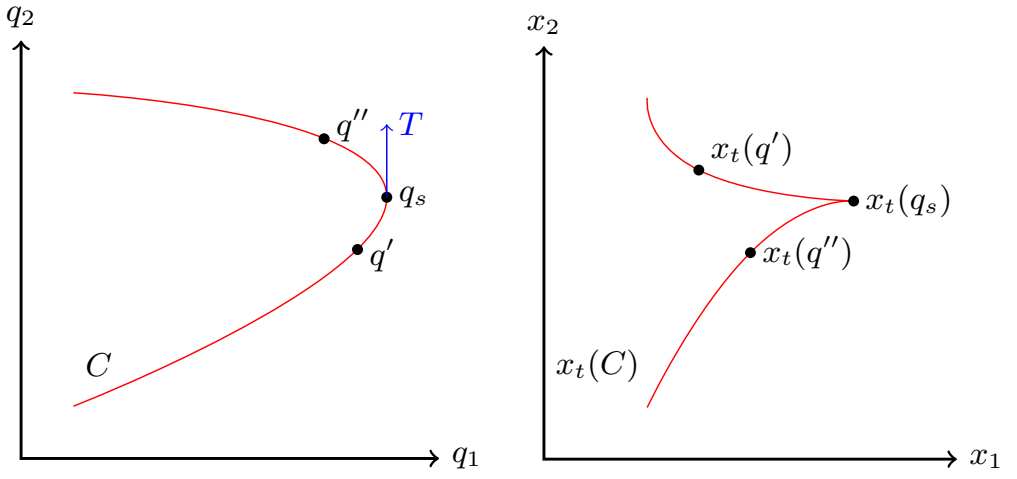

(a) Lagrangian space L (b) Eulerian space E

Figure 1: The shell-crossing process of a curve C in a Lagrangian map x_t. The left panel shows Lagrangian space, describing the initial positions of the fluid. The right panel shows Eulerian space, describing the positions of the fluid at time t. The fluid undergoes shell-crossing in point q_s on the curve C (red) at time t. The neighboring points q' and q'' have passed through the opposing segments of C. The Lagrangian mapping of the curve $x_t(C)$ (red) develops a non-differentiable point in $x_t(q_x)$, which is known as a caustic. The arrow T (blue) is the tangent vector of the curve C in point q_s.

3. Shell-crossing Conditions

The caustics mentioned above result from the folding of the fluid in phase space. At the initial time, $t = 0$, the fluid has not yet evolved. The displacement map s is therefore the zero map, i.e.,

$$s_0(q) = 0 \tag{3.1}$$

for all $q \in L$. The map $x_0(q)$ is one-to-one, i.e. each Eulerian coordinate x corresponds to one Lagrangian position q. Throughout the entire volume, the fluid only contains single-stream regions. As the fluid evolves and nonlinearities start to emerge, we see the development of *multi-stream regions* in the fluid. At the boundary of a multi-stream region, the volume of a mass element vanishes and its Lagrangian density – following eqn. 2.3 – becomes infinite. At such locations the map $x_t(q)$ attains a n-to-one character, with n an odd positive integer ($n = 3, 5, 7, \ldots$). It means that at any one Eulerian location x, streams from n different Lagrangian positions cross.

The key question we address here is that of inferring the conditions under which a mass element with Lagrangian coordinate q undergoes shell-crossing. Here we derive the necessary and sufficient conditions for the process of shell-crossing to occur. These conditions are called *shell-crossing conditions*. They are the foundation on the basis of which we infer – in section 4 – the related conditions on the displacement field for the occurrence of the various classes of caustics. These are called the *caustic conditions*. We infer the caustic conditions for generic as well as Hamiltonian fluid dynamics.

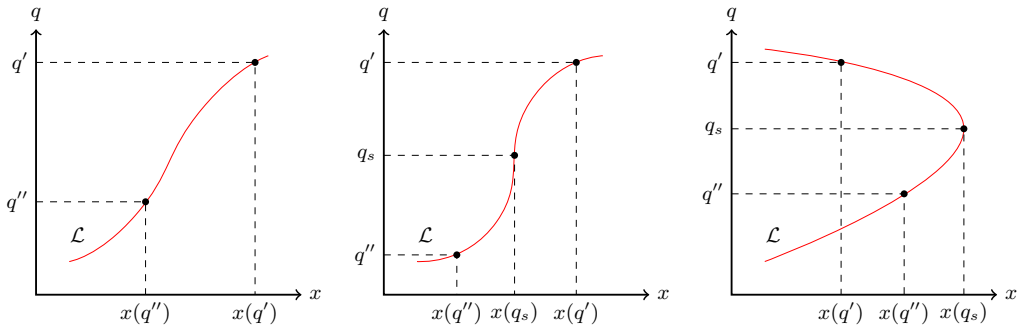

Figure 2: Folding of a one-dimensional fluid in phase space $\mathcal{C}$. The three panels show the time evolution of the Lagrangian submanifold $\mathcal{L}$ (red) of the fluid in phase space. We track the evolution of two points $(q', x(q')), (q'', x(q''))$ forming a multi-stream region and mark the point undergoing shell-crossing by $(q_s, x(q_s))$. Left panel: the fluid – early in its evolution – consisting of a single-stream region. Middle panel: a fluid during the process of shell-crossing. Right panel: a fluid consisting of a multi-stream region.

3.1. *Shell-crossing condition: the derivation*

A typical configuration resulting from the *shell-crossing process* – the name by which it is usually indicated – is illustrated in figure 1. It focuses on points $q = (q_1, q_2)$ that lie on a smooth curve C in Lagrangian space L (fig. 1a). At time t, the points on the Lagrangian curve C map to the variety $x_t(C)$ in Eulerian space E (fig. 1b). The fluid in point q_s undergoes shell-crossing at time t. The neighboring points q' and q'' have passed through the opposing segments of C. As a result of this, the curve C develops a non-differentiable point in $x_t(q_x)$, which is known as a *caustic*.

In a time sequence of three steps, figure 2 illustrates the dynamical process that is underlying the formation of the caustic at $x_t(q_s)$. The singularity at $x_t(q_s) \in x_t(C)$ forms as the result of a folding process in phase space. We may appreciate the emerging structure when assessing the fate of two neighboring points $q', q'' \in C$ on both sides of q_s. While the phase space sheet $x_t(C)$ is folded, the points $x_t(q')$ and $x_t(q'')$ turn around while passing through $x_t(q_s)$. In figure 2 we observe how the initially single-stream phase space sheet (lefthand panel) morphs into a configuration marked by shell-crossing as different mass elements q pile up at the same Eulerian position $x_t(q_s)$ (central panel). Subsequently, around $x_t(q_s)$ we notice the formation of a multi-stream region, with the presence of mass elements q' having passed into a region where mass elements from other Lagrangian locations q are to be found.

To infer the shell-crossing conditions, we investigate a curve C in Lagrangian space along which we have points q that will find themselves incorporated in a singularity at Eulerian position $x_s(q_s)$. In the case of shell-crossing, points q near the Lagrangian location q_s will map onto the same Eulerian position $x(q_s)$. The key realization is that this occurs as points q along a direction T tangential to C are all folded on to a single Eulerian position $x_s(q_s)$. This translates the question of the shell-crossing condition into one on the identity of a tangential direction $T(q)$ along which shell-crossing may or will occur. In other words, whether on a particular curve C – or, more general, a manifold M – there are points q where along one or more tangential directions $T(q)$ to that curve or manifold shell-crossing may or will take place.

Zooming in on two points q' and q'' in the vicinity of the singularity point q_s, we see that as a result of the folding process the ratio of the distances of the two points in the

Lagrangian and Eulerian manifold,

$$\frac{\Delta x}{|\Delta q|} = \frac{\|x_t(q') - x_t(q'')\|}{\|q' - q''\|} \to 0 \qquad q', q'' \to q_s \tag{3.2}$$

must go to zero in the limit that we zoom in on points q' and q'' along the Lagrangian curve C at an infinitesimal distance from q_s. The direct implication of this is, following equation 2.3, that the Lagrangian density in a caustic is infinite: the volume of the mass element associated to q_s vanishes at time t. In essence it informs us that during shell crossing the points q near Lagrangian location q_s, along the tangential direction T to the Lagrangian curve C, map onto the same Eulerian position $x(q_s)$. This means that the norm of the directional derivative of x_t along the tangential direction vanishes. In other words, along the non-zero tangent vector T along C,

$$\left\| \frac{\partial x_t}{\partial q} T \right\| = 0\,, \tag{3.3}$$

where $\partial x_t/\partial q$ is the Jacobian of x_t evaluated in q_s (see figure 1a). This is equivalent to requiring that

$$\frac{\partial x_t}{\partial q} T = 0\,. \tag{3.4}$$

In terms of the displacement map s_t, this condition can be expressed as

$$T + \frac{\partial s_t}{\partial q} T = 0\,, \tag{3.5}$$

with the Jacobian $\frac{\partial s_t}{\partial q}$ also evaluated in q_s†. Assuming the Jacobian to be diagonalizable, in which case the eigenvectors are linearly independent (which is a stronger condition then that they are non-degenerate) ‡, we may write the Jacobian in its eigendecomposition

$$\frac{\partial s_t}{\partial q} = \mathcal{M} = \mathcal{V}\mathcal{M}_d\mathcal{V}^{-1}\,. \tag{3.6}$$

In this expression, $\mathcal{M}_d$ is the diagonal matrix of the deformation tensor $\mathcal{M}$, with diagonal elements the eigenvalues μ_i,

$$\mathcal{M} v_i = \mu_i v_i\,. \tag{3.7}$$

The matrix $\mathcal{V}$ the corresponding eigenvector matrix whose columns are the corresponding eigenvectors v_i. In three dimensions, with the eigenvalues μ_i and eigenvectors $v_i = (v_{i,1}, v_{i,2}, v_{i,3})$, the diagonal matrix $\mathcal{M}_d$ and eigenvector matrix $\mathcal{V}$ are given by

$$\mathcal{M}_d = \begin{pmatrix} \mu_1 & 0 & 0 \\ 0 & \mu_2 & 0 \\ 0 & 0 & \mu_3 \end{pmatrix}, \qquad \mathcal{V} = \begin{pmatrix} v_{1,1} & v_{2,1} & v_{3,1} \\ v_{1,2} & v_{2,2} & v_{3,2} \\ v_{1,3} & v_{2,3} & v_{3,3} \end{pmatrix}, \tag{3.8}$$

with $\mathcal{M}_d$ the diagonal matrix with on the diagonal the eigenvalues μ_i and eigenvector matrix $\mathcal{V}$. In terms of $\mathcal{V}$ and $\mathcal{M}_d$, condition 3.5 reduces to

$$(I + \mathcal{M}_d)\mathcal{V}^{-1} T = 0\,. \tag{3.9}$$

Note that the rows of $\mathcal{V}^{-1}$ consist of the dual vectors $\{v_i^*\}$ of the eigenvectors $\{v_i\}$,

† Unless mentioned otherwise, we will assume all Jacobians to be evaluated in q_s.

‡ The eigenvectors are linearly dependent with measure zero, since the Jordan decomposition is unstable under small fluctuations of the matrix elements. We will always assume the Jacobian $\frac{\partial s}{\partial q}$ to be diagonalizable.

defined by $v_i \cdot v_j^* = \delta_{ij}$ for all i and j. Explicitly, this means that $\mathcal{V}^{-1}$ in three dimensions is given by

$$\mathcal{V}^{-1} = \begin{pmatrix} v_{1,1}^* & v_{1,2}^* & v_{1,3}^* \\ v_{2,1}^* & v_{2,2}^* & v_{2,3}^* \\ v_{3,1}^* & v_{3,2}^* & v_{3,3}^* \end{pmatrix}, \tag{3.10}$$

with $v_i^* = (v_{i,1}^*, v_{i,2}^*, v_{i,3}^*)$. The product $\mathcal{V}^{-1}T$ is the vector composed out of the inproduct of these dual vectors with the tangent vector T, so that in three dimensions equation 3.9 reduces to

$$\begin{pmatrix} (1+\mu_1)v_1^* \cdot T \\ (1+\mu_2)v_2^* \cdot T \\ (1+\mu_3)v_3^* \cdot T \end{pmatrix} = 0\,. \tag{3.11}$$

This represents the proof for the shell-crossing condition for one-dimensional submanifolds. It states the condition for the tangential direction T along which Lagrangian points get folded into an Eulerian singularity point. The obtained condition is a telling expression for the central role of the deformation eigenvalues in determining the occurrence of a singularity.

Note that the above is based on the key assumption that the Jacobian $\partial s/\partial q$ is diagonalizable.

3.2. *Shell-crossing condition: theorems*

Following the proof outlined in the previous subsection 3.1, we arrive at the following two theorems stipulating the conditions for the formation of singularities by curves C and arbitrary manifolds M in Lagrangian space L,

THEOREM: 1.

A smooth curve $C \subset L$ forms a singularity under the mapping x_t in the point $x_t(q_s) \in x_t(C) \subset E$ if and only if

$$(1 + \mu_{it}(q_s))v_i^*(q_s) \cdot T = 0 \tag{3.12}$$

for all i, with T a nonzero tangent vector of C in q_s.

For fluids with Hamiltonian dynamics (see sect 2.1) the Jacobian $\partial s_t/\partial q$ is symmetric. The eigenvectors of such a Jacobian can be taken to be orthonormal. The dual vectors of such a set of eigenvectors coincide with the eigenvectors, i.e. $v_i^* = v_i$.

A similar argument holds for higher dimensional submanifolds of L, e.g., sheets and volumes. These manifolds can be n-dimensional, with $n = 1, \ldots, 3$ for three-dimensional fluids. Given an arbitrary manifold $M \subset L$ we can consider all curves $C \subset M$ passing through the point $q_s \in M$. The variety $x_t(M)$ contains a singularity at $x_t(q_s)$ if and only if at least one such curve $C \subset M$ gets folded under the map x_t. Hence for an arbitrary submanifold M, we should consider the one-dimensional shell-crossing condition for all

tangent vectors T in the vector space $T_{q_s}M$ of all tangential vectors to the manifold M in $q_s \in M$ †. This proves the general shell-crossing condition:

THEOREM: 2.

A manifold $M \subset L$ forms a singularity under the mapping x_t in the point $x_t(q_s) \in x(M,t) \subset E$ at time t if and only if there exists at least one nonzero tangent vector $T \in T_{q_s}M$ satisfying

$$(1 + \mu_i(q_s))v_i^*(q_s) \cdot T = 0 \tag{3.13}$$

for all i.

3.3. *Shell-crossing conditions: significance*

The shell-crossing conditions, as expressed in the two theorems above, are in agreement with our observation in section 2. That is, the conditions express the fact that caustics satisfy the sufficient and necessary condition $1 + \mu_i = 0$ for at least one i.

This conclusion follows from the observation that if indeed at least for one i we have that $1+\mu_i = 0$, we can always choose the vector T orthogonal to the span of eigenvectors $\{v_j | j \neq i\}$. For example, for the three-dimensional situation: if $1 + \mu_1 = 0$, we may chose the vector T to be orthogonal to the plane defined by the eigenvectors v_2 and v_3. Along the direction of T we see the Lagrangian points q end up in a singularity in the Eulerian location $x(q_s)$. Overall, the eigenvalue condition $1 + \mu_i = 0$ defines a two-dimensional sheet in Lagrangian space. This sheet forms a singularity, containing points q that function as singularity points. If, however, both $1+\mu_1 = 0$ and $1+\mu_2 = 0$, then T will be a vector orthogonal to the eigenvector v_3. The eigenvalue conditions define a line through three-dimensional Lagrangian space, the points q along which are singularity points. Conversely, if $1 + \mu_i \neq 0$ for all i, then there does not exist a T satisfying the general shell-crossing condition.

3.4. *Shell-crossing conditions: coordinate transformation*

The shell-crossing conditions are manifestly independent of coordinate choices. However, the eigenvalues and eigenvector fields generally do depend on the choice of coordinates. By themselves, they do therefore not provide valid descriptions of the dynamics of the fluid. Suppose the displacement field can be written as $s = \nabla\psi$ for some potential ψ. The Hessian H_x of ψ,

$$H_{ij} \;=\; \frac{\partial^2\psi}{\partial x_i \partial x_j}\,, \tag{3.14}$$

non-trivially transforms under the local coordinate transformation $x \to X(x)$ as $H \to \tilde{H}$ according to

$$\tilde{H} \;=\; J^T H J + J^T \nabla(J) \nabla\psi\,, \tag{3.15}$$

† $T_{q_s}M$ is the vector space of all tangential vectors to the manifold M in $q_s \in M$.

with the J the Jacobian between the coordinate systems X and x,

$$J_{ij} \;=\; \frac{\partial X_i}{\partial x_j}\,. \tag{3.16}$$

From this we immediately infer that the eigenvalue field and eigenvector fields are invariant if the transformation is orthogonal and global, i.e. if $J^T = J^{-1}$ and $\nabla(J) = 0$. As may be expected, these transformations include rotations.

4. Caustic conditions

In the previous section 3, we inferred the general condition for shell-crossing. The condition establishes the relation between the fields of deformation tensor eigenvalues in Lagrangian space, and the Lagrangian regions that get incorporated, in Eulerian space, in features of infinite density.

On the basis of the shell-crossing condition we are able to identify a Lagrangian region that gets incorporated in a caustic. Moreover, it allows us to establish the identity of the resulting singularity in Eulerian space and its relationship to the deformation tensor eigenvalue and eigenvector fields. The stable singularities that may emerge in generic fluids or in Hamiltonian fluids, can be classified in two series, the A_k and D_k series †. The shell-crossing conditions states that a necessary and sufficient condition for the generation of caustics is that $1 + \mu_i = 0$ for at least one i. The A_k family of caustics are the ones for which this conditions holds for only one eigenvalue. Caustics for which two eigenvalues simultaneously satisfy this condition belong to the D family. In three-dimensional fluids, the case in which all eigenvalues simultaneously satisfy this condition is non-degenerate. They belong to the E family. However, we will not discuss them in the context of the present paper. In section 5, we will describe these series of caustics in more detail.

While already using the terminology of the A_k and D_k classification of singularities, the purpose of the caustic conditions inferred in this section is precisely to establish the foundation on which to base this classification. Along with a detailed description of the classification, this will be the task of next section 5 by connecting the caustic conditions to the classification of stable singularities.

In this section we restrict ourselves to the three-dimensional situation. Within 3-D space we seek to identify and qualify the Lagrangian regions that get folded into A_k or D_k singularities. As one may readily infer from the shell-crosssing conditions, this is determined by the spatial characteristics of the deformation tensor eigenvalue and eigenvector fields in Lagrangian space. The conditions that are inferred from this analysis for caustics in Lagrangian fluids are called the *caustic conditions*.

With the purpose to provide a guide that evokes a visual intuition for the connection between the structure and geometry of the eigenvalue fields and the formation of the various singularities, in particular those of the A-family, we include figure 3. It shows a contour map representing the typical structure of the eigenvalue field μ_i. This field corresponds to a two-dimensional Gaussian random density field. For reasons of convenience, we have assumed higher eigenvalues to correspond to earlier collapse, and negative ones to no collapse (in other words, we have mirrored μ_i). The geometry and topology of the eigenvalue landscape is decisive for the occurrence of singularities. This may already be inferred from the positions of different A-family singularity points and varieties, whose positions are indicated on the contour map.

† The classification ultimately has its origin in the classification of Coxeter groups

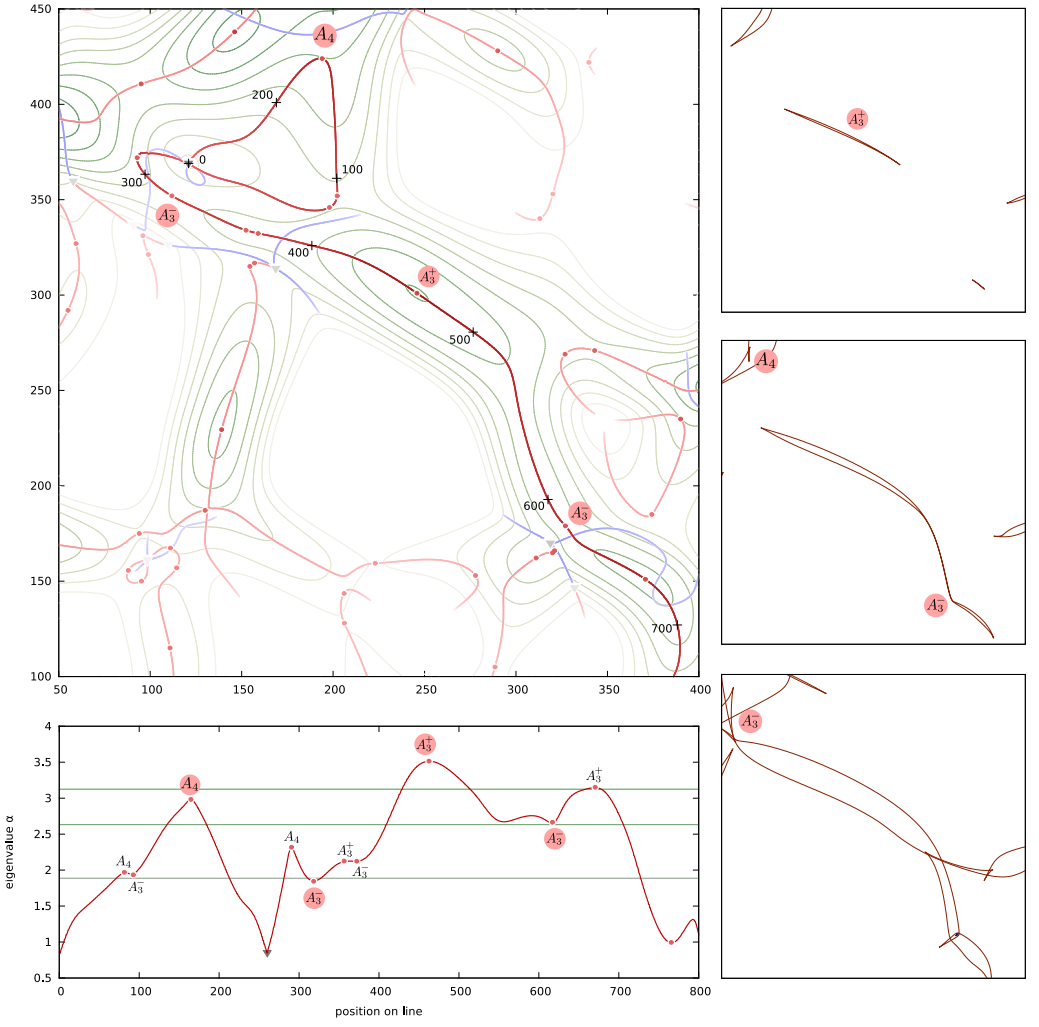

Figure 3: Eigenvalue field and singularity points. Top lefthand frame: the contour map illustrates the typical structure of the eigenvalue field corresponding to a 2-D Gaussian random density field. Indicated are the positions of different A-family singularity points and varieties. In particular noteworthy is the run of the A_3 line, which defines the ridge along which we may identify a range of A singularities. One may keenly appreciate how the identity of the various singularities is determined by the specific geometric character of the eigenvalue field $\mu(q)$, as expressed in its gradient $\nabla\mu(q)$ and higher order gradients. Bottom lefthand frame: the panel depicts the run of the eigenvalue field along the A_3 curve (in the contour map of top lefthand frame). Note the location of the $A_3^\pm$ points and A_4 points on the extrema of the curve. Righthand panels: the three panels show the evolution, in Eulerian space, of the A_3 line, according to the linear Lagrangian Zel'dovich approximation (Zel'dovich 1970). Note the appearance of the corresponding caustics and the relation between the geometry of the A_3 line in Eulerian space and the $A_3^\pm$ and A_4 points.

The landscape defined by the eigenvalue contours is varied, characterized by several peaks, connected by ridges with lower μ_i values. These, in turn, are connected to valleys in which μ_i attains negative values that will prevent collapse - along the direction of the eigenvector v_i - of the corresponding mass elements at any time. From the Lagrangian density relation (eqn. 2.4), we know that the region of space that has undergone collapse before the current epoch (i.e. attained an infinite density) is the superlevel set of the eigenvalue field defined by the current value μ_{ti}. For each time t, the positive value contours correspond to the $A_2(t)$ fold sheets. Collapse occurs first at the maxima in the field. These mark the birth of new features, and are designated by the label of A_3^+ points. Evidently, the steepness of the hill around these maxima, i.e. the gradient $\nabla\mu(q)$, will determine how and which mass elements around the hill will follow in outlining the emerging feature around the A_3^+ points.

In particular noteworthy is the run of the A_3 line. The key significance of the A_3 curve is evident from the observation that all A-family singularities are aligned along the ridge. In two-dimensional space, the A_3 curves delineate the points where the eigenvalues μ_i are maximal along the direction of the corresponding local eigenvector. At these points, along the eigenvector direction, the gradient of the eigenvalues is zero, i.e. they are the points where the eigenvector n is perpendicular to the local gradient of $\nabla\mu_i$ of the eigenvalue field. Below, in section 4.1.3, we will see that this follows directly from the shell-crossing conditions that were derived in the previous section. Because of this there is a line-up and accumulation of neighbouring mass elements that simultaneously pass through the singularity. When mapped to Eulerian space, this evokes the formation of an A_3 cusp.

To illustrate the connection between A_3 curves and the various singularities even more strongly, the bottom lefthand panel depicts the run of the eigenvalue field along the A_3 curve. In particular noteworthy is the location of the $A_3^\pm$ points and A_4 points on the extrema of the curve. A prominent aspect of this is the presence of the A_3^- points at saddle junctions in the eigenvalue field. These are topologically the most interesting locations, as they evoke the merging of separate fold sheets into a single structure. In other words, they are the points where the topological structure of the field undergoes a transition and where the connectivity of the emerging structural features is established. To establish this even more strongly, the three righthand panels of figure 3 represent a time sequence of the evolving structure along the A_3 line as it is mapped to its appearance in Eulerian space. The evolution follows the linear Lagrangian Zel'dovich approximation (see Zel'dovich (1970) and appendix A). We may note the appearance and merging of the corresponding caustics.

In all, one may keenly appreciate how the identity of the various singularities is determined by the specific geometric character of the eigenvalue field $\mu(q)$, as expressed in its gradient $\nabla\mu(q)$ and higher order gradients. In the following subsections, we will systematically inventorize the families of singularities on the basis of the shell-crossing conditions that we inferred before, and observe the connection between the singularities and the geometry of the eigenvalue field.

4.1. *The A family*

The A family of caustics form when

$$\begin{aligned} 1+\mu_i &= 0\,, \\ 1+\mu_k &\neq 0 \quad \text{for} \quad k\neq i\,, \end{aligned} \tag{4.1}$$

for some i. In other words, the caustics correspond to one eigenvalue field. In this case, the eigenvector fields $\{v_i\}$ and its dual vector fields $\{v_i^*\}$ are linearly independent. In addition, we may assume the eigenvalue fields to be sufficiently differentiable.

In total, we may identify 5 different A classes. These run from the trivial A_1 class, corresponding to the points that never form caustics, to the highest dimensional A singularity class, the A_5 butterfly caustics. The A family includes the sheetlike A_2 fold singularities, the curvelike A_3 cusp singularities, the A_4 swallowtail singularities and the A_5 butterfly singularity.

4.1.1. *The trivial A_1 class*

The A_1 class labels the points which never form caustics.

According to the shell-crossing condition, q_s will form a singularity at time t if and only if there exists a nonzero tangent vector $T \in T_{q_s}L$ for which

$$(1 + \mu_i(q_s))v_i^*(q_s) \cdot T = 0 \tag{4.2}$$

for all i. The point q_s will not satisfy this condition if $1 + \mu_i(q_s) \neq 0$ for all i since the three dual vectors $\{v_i^*\}$ span the tangent space $T_{q_s}L$.

From the shell-crossing condition we therefore conclude that the three-dimensional variety A_1,

$$A_1 = \{q \in L | 1 + \mu_{ti}(q) \neq 0 \text{ for all } i \text{ and } t\}, \tag{4.3}$$

consists of the points never forming caustics. In this respect we should note that the displacement map at the initial time is the zero map, so that the eigenvalues at the initial time are equal to zero, i.e. $\mu_{0i}(q) = 0$ for all $q \in L$. Since the eigenvalues are continuous function of time, the requirement for a point q to belong to A_1 is equivalent to $\mu_{ti}(q) > -1$.

4.1.2. *The A_2 caustics*

Based on the discussion above, we may conclude that for a given i, $i = 1 \ldots 3$, at time t the points

$$A_2^i(t) = \{q \in L | 1 + \mu_{ti}(q) = 0\} \tag{4.4}$$

form a singularity. For three-dimensional fluids, the set $A_2(t)$ forms a two-dimensional sheet, sweeping through space as the fluid evolves. These singularities can be associated to the A_2 fold singularity class.

From this, we conclude that the set of points which form a A_2 fold singularity at a time $t \in [0, \infty)$ is given by

$$A_2^i = \{q \in L | 1 + \mu_{ti}(q) = 0 \text{ for some } t\}. \tag{4.5}$$

4.1.3. *The A_3 caustics*

Following up on the folding of the fluid to the A_2^i singularity, the A_2^i manifold itself may actually be folded into a more complex configuration. The result is a so-called A_3 singularity. To guide understanding in the emergence of cusps we may refer to figure 4.

To infer the identity of the A_3^i caustic, we restrict the criterion for shell-crossing to points on the A_2^i manifold. In other words, we look for points q_s on the surface of the sheetlike variety $A_2^i(t)$ that fulfill the criterion for shell-crossing.

A point $q_s \in A_2^i(t)$ forms a singularity if there exists a nonzero tangent vector T, $T \in T_{q_s}A_2^i(t)$, orthogonal to the span$\{v_j^* | j \neq i\}$. This condition is satisfied if and only

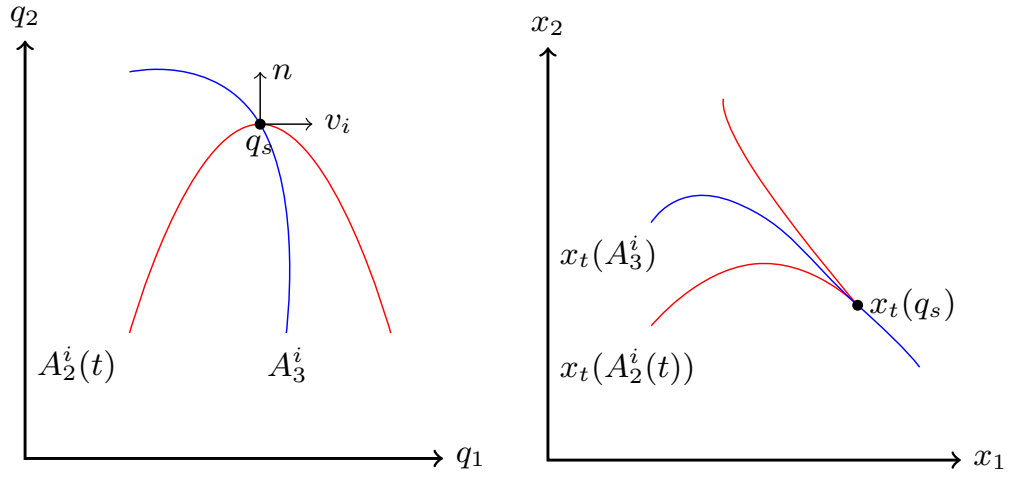

(a) Lagrangian space (b) Eulerian space

Figure 4: The formation of a cusp (A_3) singularity in a Lagrangian map x_t. The left panel shows Lagrangian space, describing the initial positions of the fluid. The right panel shows Eulerian space, describing the positions of the fluid at time t. The fluid undergoes shell-crossing along the fold $A_2^i(t)$ (red) at time t. The fold gets mapped under the Lagrangian map to $x_t(A_2)$ (red), which is folded into a cusp in the point $x_t(q_s)$ corresponding to q_s. The cusp forms if and only if the normal n of $A_2^i(t)$ is orthogonal to the eigenvector field v_i in q_s. Over time, the cusp traces out the curve A_i (blue) which is mapped to $x_t(A_3^i)$ (blue).

if the tangent vector T is parallel to v_i. This is equivalent to the condition that v_i is orthogonal to the normal $n = \nabla\mu_{ti}$ of the manifold $A_2^i(t)$ in the point q_s. Explicitly, this means that the inproduct of n with v_i is equal to 0,

$$\mu_{ti,i} \equiv v_i \cdot \nabla\mu_{ti} = 0\,. \tag{4.6}$$

The points q forming a cusp at time t therefore represent the one-dimensional variety defined by

$$A_3^i(t) = \{q \in L | q \in A_2^i(t) \ \wedge \ \mu_{ti,i}(q) = 0\}\,. \tag{4.7}$$

Extrapolating this to the set of all points q that at some time $t \in [0, \infty)$ have belonged to or will be incorporated in a cusp singularity defines a two-dimensional variety

$$A_3^i = \{q \in L | q \in A_2^i(t) \ \wedge \ \mu_{ti,i}(q) = 0 \text{ for some } t\}\,, \tag{4.8}$$

which is the assembly of all $A_3^i(t)$ over the time interval $t \in [0, \infty)$.

4.1.4. *The $A_3^{\pm}$ points*

The topology of the sheetlike $A_2^i(t)$ variety changes as a function of time. These topological changes occur at critical points of the corresponding eigenvalue field μ_{ti}. It is at these points where in Eulerian space we see the emergence of new features, the disappearance of features and/or the merging of features. The critical points are classified as cusp singularities.

At minima of the μ_i field, a feature gets created. At maxima, a feature gets annihilated.

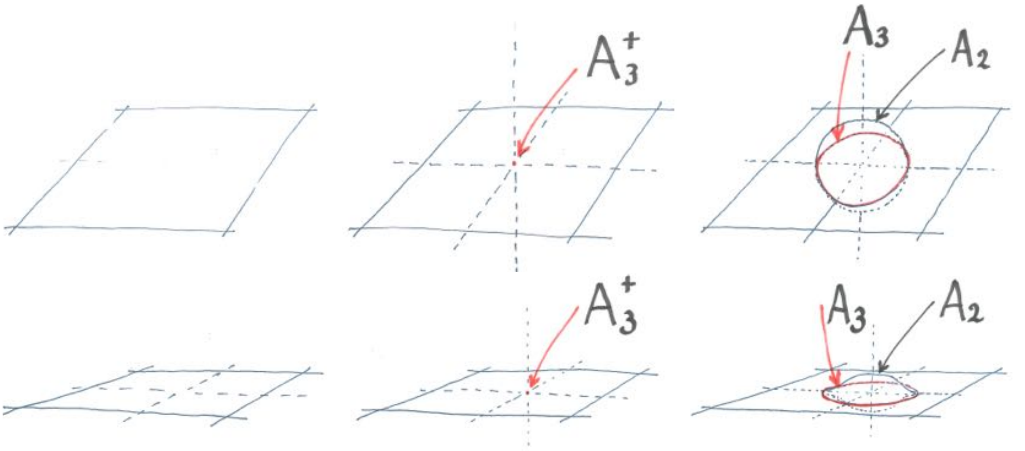

Figure 5: The creation/annihilation of a fold (A_2) sheet in a A_3^+ point. The upper three panels show the unfolding of a A_3^+ singularity in Lagrangian space. The lower three panels show the corresponding unfolding in Eulerian space. The two panels on the left show the cusp (A_3) plane on which the cusps form. The middle panels show the appearance of a A_3^+ singularity in which a fold sheet is formed/removed. The right panels show the resulting fold (A_2) sheet. The fold sheet gets folded into a cusp (A_3) curve (red). This configuration is known as the *Zel'dovich pancake* (Zel'dovich 1970).

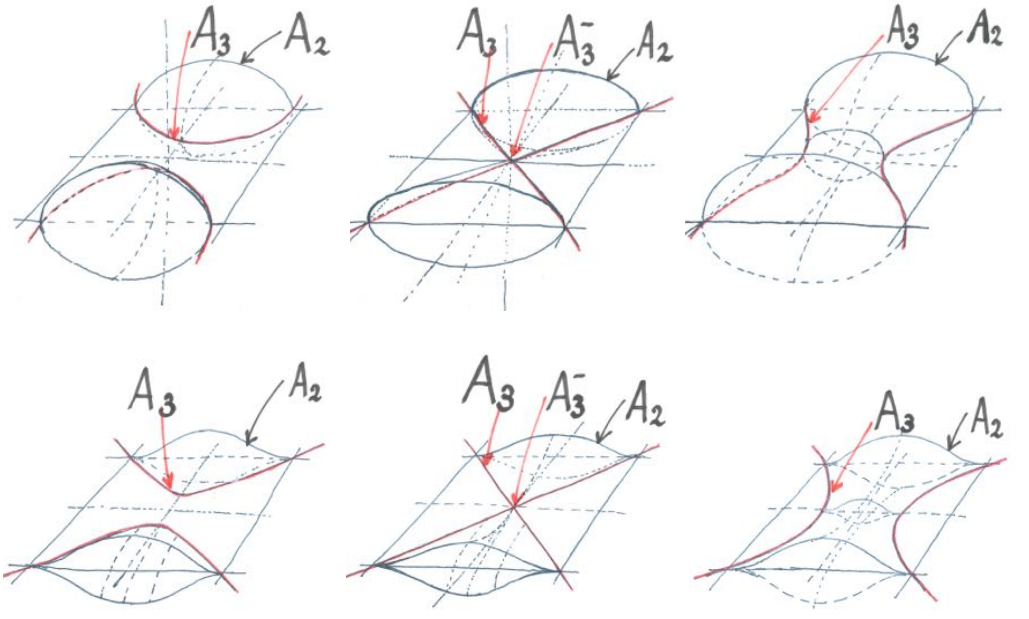

Figure 6: The merger/splitting of a fold (A_2) sheet in a A_3^- point. The upper three panels show the unfolding of a A_3^- singularity in Lagrangian space. The lower three panels show the corresponding unfolding in Eulerian space. The two panels on the left show two fold (A_2) sheets, two cusp (A_3) curves (red) and the cusp (A_3) plane on which the cusps form. The middle panels show the merger/splitting of the two fold (A_2) sheets in a A_3^- singularity. The right panels show the resulting merged fold (A_2) sheet. This configuration is known as the *Kissing Lips*.

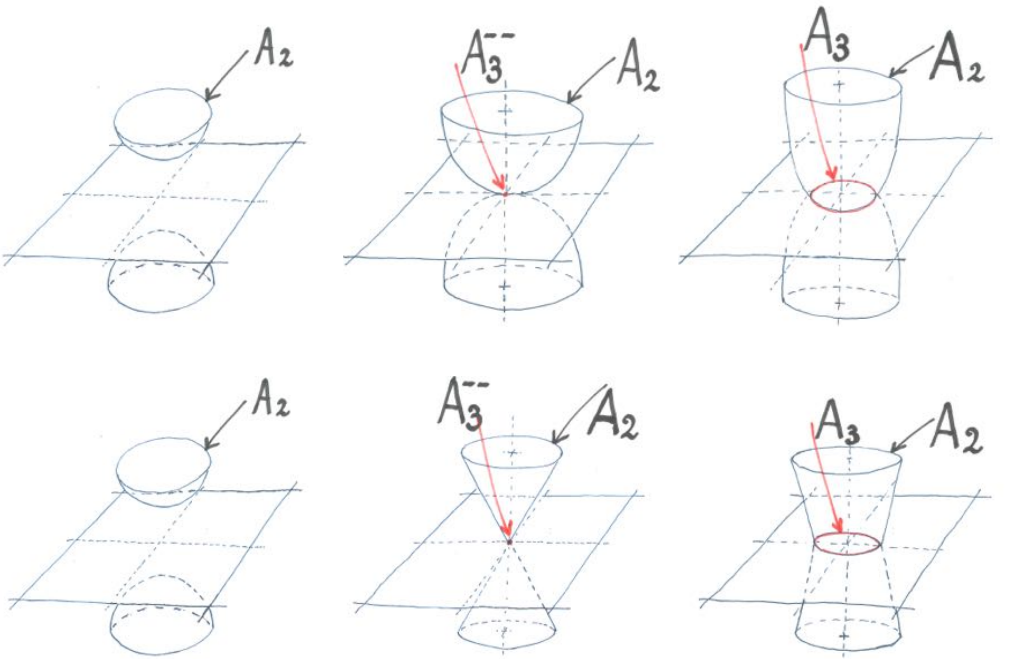

Figure 7: The merger/splitting of a fold (A_2) sheet in a A_3^{--} point. The upper three panels show the unfolding of a A_3^{--} singularity in Lagrangian space. The lower three panels show the corresponding unfolding in Eulerian space. The two panels on the left show two fold (A_2) sheets, and the cusp (A_3) plane on which the cusps form. The middle panels show the merger/splitting of the two fold (A_2) sheets in a A_3^{--} singularity. The right panels show the resulting merged fold (A_2) sheet with the corresponding cusp (A_3) curve.

Particularly interesting points are the saddle points. In three-dimensional space, there are two classes of saddles in the eigenvalue field μ_{ti}. The index 1 saddles have a Hessian signature $(--+)$, with 1 positive eigenvalue, while the index 2 saddles have a signature $(-++)$.

Based on their impact on caustic structure, Arnol'd used a slightly different classification scheme, in which the distinguished between A_3^{++}, A_3^{+-} and A_3^{--} points (Arnol'd 1982). The A_3^{++} point are identified with the minima†, while the A_3^{+-} points are the saddle points for which the A_3 sheet intersects the two disjoint A_2 sheets. This is illustrated in the upper left panel in figure 6. The additional A_3^{--} points correspond to saddle points for which the A_3 sheet does not intersect the disjoint A_2 sheets. Because this concerns a non-generic situation, we do not treat it here. Also note that higher dimensional fluids will have additional A_3 points.

In the context of this paper we therefore use a slightly shorter notation for the maxima, minima and saddles, classifying them as the cusp singularities A_3^+ an A_3^-,

$$\begin{aligned} A_3^{i+} &= \{q \in L | q \in A_2^i(t) \wedge \mu_{ti}(q) \text{ max-/minimum of } \mu_{ti} \text{ at some time } t\}\,, \\ A_3^{i-} &= \{q \in L | q \in A_2^i(t) \wedge q \text{ saddle point of } \mu_{ti} \text{ at some time } t\}. \end{aligned} \tag{4.9}$$

† Note that in Arnol'ds notation, related to the Zel'dovich formalism (see appendix A), these are the maxima of the eigenvalue field

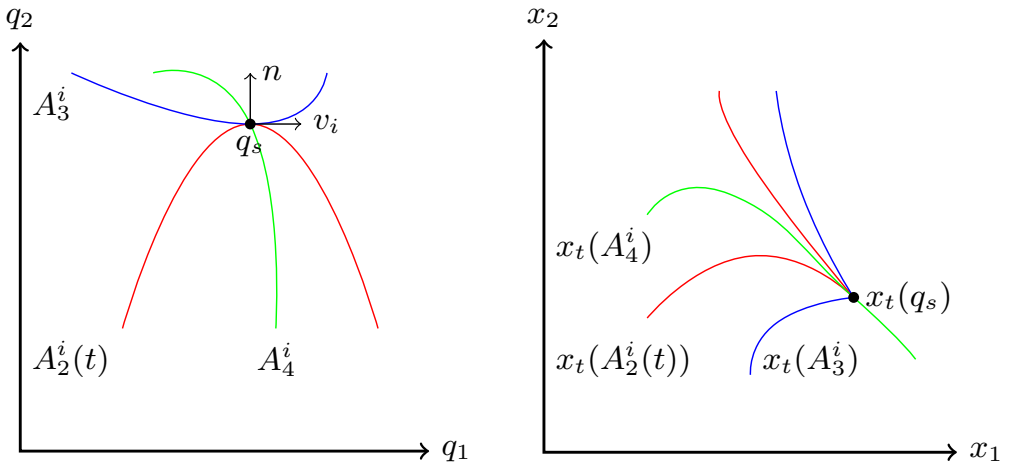

(a) Lagrangian space

(b) Eulerian space

Figure 8: The formation of a swallowtail (A_4) singularity in a Lagrangian map x_t. The left panel shows the Lagrangian space describing the initial positions of the fluid. The right panel shows the Eulerian space describing the positions of the fluid at time t. The fluid undergoes shell-crossing along $A_2^i(t)$ (red) at time t. The fold gets mapped in Eulerian space, under the Lagrangian map, to $x_t(A_2)$ (red), which is folded into a cusp in the point $x_t(q_s)$ corresponding to q_s. The cusp forms if and only if the normal n of $A_2^i(t)$ is orthogonal to the eigenvector field v_i in q_s. Over time, in Lagrangian space the cusp traces out the curve A_i (blue) which in Eulerian space is mapped to $x_t(A_3^i)$ (blue). Since the cusp (A_3^i) curve is tangential to the fold (A_2) curve in q_s, the cusp curve $x_t(A_3^i)$ forms a swallowtail (A_4) singularity. Over time, the swallowtail traces out A_4^i (green), which in Eulerian space is mapped into $x_t(A_4^i)$ (green).

Note that in this scheme, the saddle points with index 1 and 2 belong to the same singularity class A_3^{i-}. For an illustration of the A_3^+ and A_3^- singularities, we refer to figures 5 and 6. From the caustics conditions we may directly infer that the $A_3^{i\pm}$ points are located on the A_3^i variety.

4.1.5. *The A_4 caustics*

In Eulerian space the $A_3^i(t)$ variety gets folded in points associated with A_4 swallowtail singularities.

The identity of the points defining the variety $A_4^i(t)$ can be inferred by the application of the general shell-crossing condition (eqn. 3.13) to the point set defining the $A_3^i(t)$ variety (see figure 8). On the basis of this, the A_4^i identity is defined as

$$A_4^i(t) = \{q \in L | q \in A_3^i(t) \wedge \mu_{ti,ii}(q) = 0\}, \tag{4.10}$$

with $\mu_{ti,ii}(q)$ the inproduct of the normal $n = \nabla\mu_{ti,i}$ with the eigenvector v_i,

$$\mu_{ti,ii} \equiv v_i \cdot \nabla\mu_{ti,i}\,. \tag{4.11}$$

Integrated over time, the points on the varieties $A_4^i(t)$ trace out the 1-dimensional variety A_4^i, i.e. the 1D line A_4^i is the set of all points $A_4^i(t)$ over the time interval $t \in [0, \infty)$,

$$A_4^i = \{q \in L | q \in A_3^i(t) \wedge \mu_{ti,ii}(q) = 0 \text{ for some } t\}\,. \tag{4.12}$$

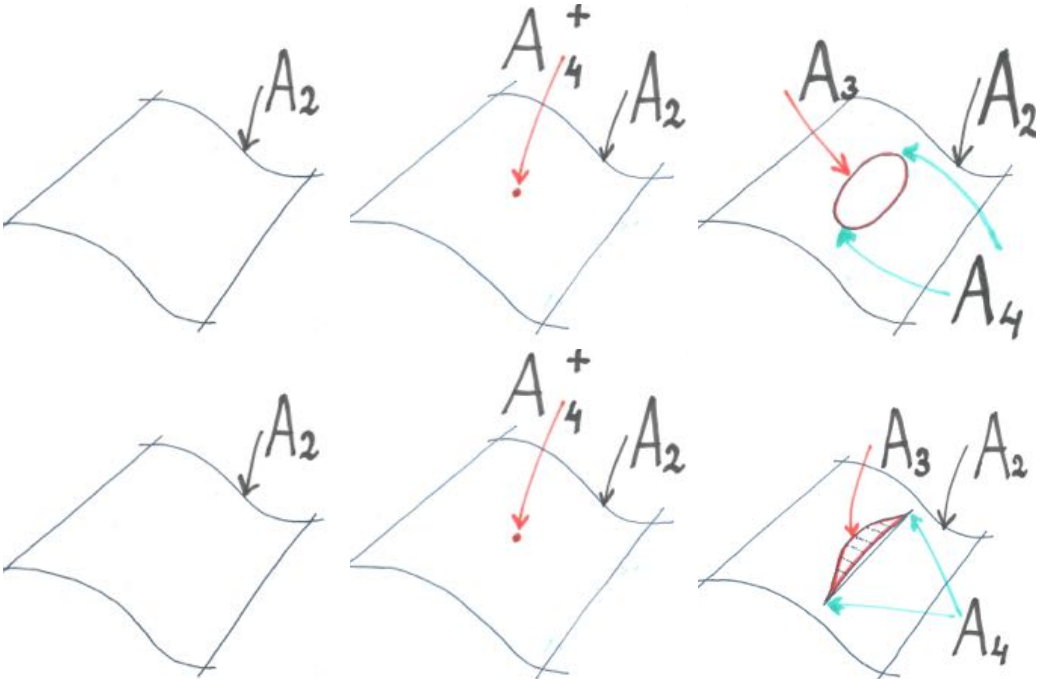

Figure 9: The creation/annihilation of a swallowtail (A_4) singularity in a A_4^+ point. The upper three panels show the unfolding of a A_4^+ singularity in Lagrangian space. The lower three panels show the corresponding unfolding in Eulerian space. The two panels on the left show a fold (A_2) sheet. The middle panels show a A_4^+ point on the fold (A_2) sheet. The A_4^+ point leads to the creation/annihilation of two swallowtail (A_4) singularities. The right panels show the resulting cusp (A_3) curves and swallowtail (A_4) singularities.

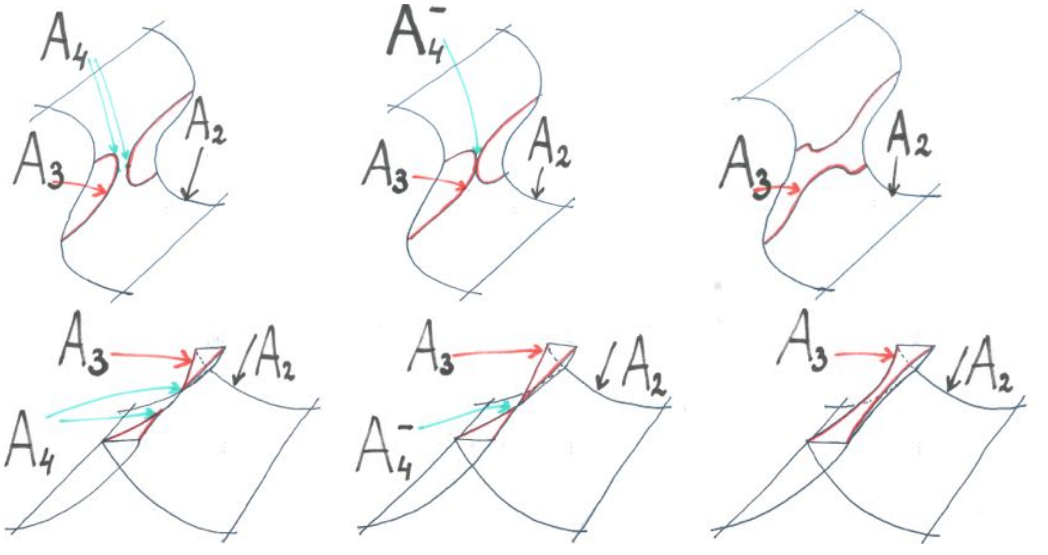

Figure 10: The merger/splitting of a cusp (A_3) curve in a A_4^- point. The upper three panels show the unfolding of a A_4^- singularity in Lagrangian space. The lower three panels show the corresponding unfolding in Eulerian space. The two panels on the left show a fold (A_2) sheet, cusp (A_3) curves and swallowtail (A_4) singularities. The middle panels show the merger/splitting of the cusp (A_3) curves in a A_4^- point. The right panels show the resulting fold (A_2) sheet and cusp (A_3) curves singularities.

4.1.6. *The $A_4^{\pm}$ points*

Also the topology of the variety $A_3^i(t)$ changes as a function of time. To this end, we identify the critical points of the field $\mu_{i,i}$,

$$\mu_{ti,i} \equiv v_i \cdot \nabla \mu_{ti} \,. \tag{4.13}$$

Constraining the location of these singularities to the one-dimensional curvelike variety $A_3^i(t)$, and thus implicitly also to the two-dimensional membrane of the variety $A_2^i(t)$, these $A_4^{\pm}$ points mark the locations at which topological changes occur. They represent the sites at which we see the birth of new singularities in Eulerian space, or the annihilation of and/or merging of such features. These singularities are classified as swallowtail singularities.

The birth or death of features on $A_3^i(t)$ takes place at maxima and minima of $\mu_{ti,i}$, and is identified with A_4^{i+} singularities. The merging or splitting of features happens at the saddle points of the same field $\mu_{ti,i}$. The latter mark the A_4^{i-} singularities,

$$\begin{aligned} A_4^{i+} &= \{q \in L | q \in A_3^i(t), \mu_{ti,i}(q) \text{ max-/minimum of } \mu_{ti,i}|_{A_2^i(t)} \text{ for some } t\}, \\ A_4^{i-} &= \{q \in L | q \in A_3^i(t) \text{ saddle point of } \mu_{ti,i}|_{A_2^i(t)} \text{ for some } t\}. \end{aligned} \tag{4.14}$$

The $A_4^{\pm}$ critical points are constrained to lie on the curvelike variety $A_2^i(t)$. Their identity is therefore determined by the interplay between the geometric properties of two entities. One of these is the geometry of the field $\mu_{ti,i}$, the other that of the geometry of the curvelike variety $A_3^i(t)$. For illustrations of the A_4^+ and A_4^- singularities we refer to figure 9 and 10.

From the caustic conditions – as expressed in eqn. 4.10 – we may also immediately observe that the $A_4^{i\pm}$ points belong to the A_4^i variety. In fact, this also represents a condition on the topology of the field $\mu_{ti,i}$ and that of the $A_2^i(t)$ variety.

4.1.7. *The A_5 caustics*

Finally, also the swallowtail curves A_4^i curve get folded in Eulerian space. It leads to the emergence of so-called butterfly singularities, or A_5 singularities. Following the same reasoning as for the A_3^i and A_4^i varieties, we may infer from the general shell-crossing condition that the A_4^i curve gets folded in the points,

$$A_5^i = \{q \in L | q \in A_4^i(t) \text{ and } \mu_{ti,iii} = 0 \text{ for some time } t\}. \tag{4.15}$$

Figure 11 shows an illustration of a A_5 singularity.

The butterfly singularity is the highest dimensional singularity that may surface in three-dimensional Lagrangian fluids. It is important to realize that the butterfly singularity only exists at one point in space-time.

4.2. *The D family*

The D family of caustics correspond to manifolds for which the caustic conditions holds for two eigenvalue fields simultaneously,

$$\begin{aligned} 1 + \mu_i &= 0 \,, \\ 1 + \mu_j &= 0 \,, \quad \text{for} \quad j \neq i \\ 1 + \mu_k &\neq 0 \,, \quad \text{for} \quad k \neq i, j \,. \end{aligned} \tag{4.16}$$

From this, we may immediately infer that these caustics form at the intersection of two $A_2(t)$ fold sheets, the $A_2^i(t)$ and $A_2^j(t)$ varieties. In all, 2 families of D caustics can be

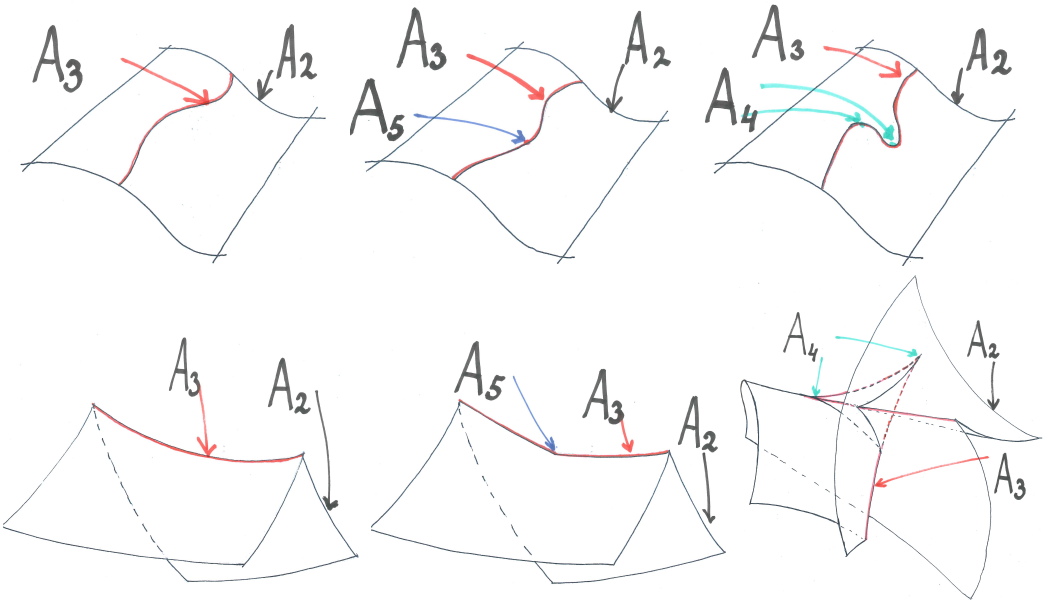

Figure 11: The creation/annihilation of swallowtail singularities in a butterfly (A_5) singularity. The upper three panels show the unfolding of a A_5 singularity in Lagrangian space. The lower three panels show the corresponding unfolding in Eulerian space. The two panels on the left show a fold (A_2) sheet, and cusp (A_3) curve. The middle panels show the creation/annihilation of the butterfly (A_5) singularity on the cusp (A_3) curve. The right panels show the resulting fold (A_2) sheet, cusp (A_3) curve and swallowtail (A_4) singularities.

identified, the D_4 elliptic and hyperbolic umbilic caustics and the D_5 parabolic umbilic caustic.

4.2.1. *The D_4 caustics*

The D_4 caustics are defined by the points q in Lagrangian space, at which two of the eigenvalues have the same value. For instance, the $D_4^{ij}(t)$ caustic, with $i \neq j$, is outlined by the points q for which at the time t the eigenvalues μ_i(t) and $\mu_j(t)$ are equal, $\mu_{ti} = \mu_{tj}$. While the eigenvalue μ_{ti} defines the fold sheet A_2^i, and the eigenvalue μ_{ti} the fold sheet A_2^j, the umbilic D_4^{ij} caustic consist of the set of points q for which

$$D_4^{ij}(t) = \{q \in L | q \in A_2^i(t) \cap A_2^j(t)\}\,. \tag{4.17}$$

In three-dimensional space, one would expect that the intersection of the two sheets $A_2^i(t)$ and $A_2^j(t)$ to consist of one-dimensional curves. This would certainly be true for two sheets that would be entirely independent of each other. However, the situation at hand concerns a highly constrained situation, in which the two eigenvalues μ_i and μ_j are strongly correlated.

Because of the latter, the intersection between the folds A_2^i and A_2^j is considerably more complex. Instead of a continuous curve, the intersection consists of isolated, singular points. A telling illustration – and discussion – of this, for the two-dimensional situation, can be found in Hidding *et al.* (2014).

The D_4 equation

To investigate the geometry and structure of the set $D_4^{ij}(t)$ we focus on the particular situation of the set $D_4^{12}(t)$, in which the two first eigenvalues μ_1 and μ_2 have the same value, $\mu_{t1} = \mu_{t2}$. Without loss of generality, we transform the coordinate system such that the third eigenvector v_3 defines the q_3 axis. This transformation makes the q_1q_2-plane the one in which we see the folding and collapse of the phase space sheets to the A_2^1 and A_2^2 caustics. In this coordinate system, the deformation tensor $\mathcal{M}$ has the form

$$\mathcal{M} = \begin{pmatrix} M_{11} & M_{12} & 0 \\ M_{12} & M_{22} & 0 \\ 0 & 0 & \mu_3 \end{pmatrix}, \tag{4.18}$$

in which μ_3 is the third eigenvalue of $\mathcal{M}$. The eigenvalues μ_1, μ_2 and μ_3 are obtained from the resulting characteristics polynomial,

$$\begin{aligned} \chi(\mu) &= \mathcal{M} - \mu I \\ &= \left[\mu^2 - \mathrm{Tr}(\tilde{\mathcal{M}})\,\mu + \det(\tilde{\mathcal{M}})\right](\mu_3 - \mu) = 0\,. \end{aligned} \tag{4.19}$$

in which the $\tilde{\mathcal{M}}$ is the $\{12\}$-submatrix of the deformation tensor,

$$\tilde{\mathcal{M}} = \begin{pmatrix} M_{11} & M_{12} \\ M_{12} & M_{22} \end{pmatrix}, \tag{4.20}$$

with trace $\mathrm{Tr}(\tilde{\mathcal{M}})$ and determinant $\det(\tilde{\mathcal{M}})$,

$$\begin{aligned} \mathrm{Tr}(\tilde{\mathcal{M}}) &= M_{11} + M_{22}\,, \\ \det(\tilde{\mathcal{M}}) &= M_{11}M_{22} - M_{12}^2\,. \end{aligned} \tag{4.21}$$

Solving the characteristic polynomial equation yields for the first two eigenvalues μ_1 and μ_2,

$$\mu_{1,2} = \frac{1}{2}\left(\mathrm{Tr}(\tilde{\mathcal{M}}) \pm \sqrt{\mathrm{Tr}(\tilde{\mathcal{M}})^2 - 4\det(\tilde{\mathcal{M}})}\right), \tag{4.22}$$

while, evidently, the third eigenvalue is μ_3. For the particular situation of the D_4^{12} caustic, we know that $1 + \mu_1 = 1 + \mu_2 = 0$, and hence that $\mu_1 = \mu_2 = \mu$ (see eqn. 4.16). This translates into the the condition that

$$\mathrm{Tr}(\tilde{\mathcal{M}})^2 = 4\det\tilde{\mathcal{M}}\,. \tag{4.23}$$

Expressed in terms of the $\tilde{\mathcal{M}}$ matrix elements, this condition translates into

$$(M_{11} - M_{22})^2 + 4M_{12}^2 = 0\,, \tag{4.24}$$

from which we obtain the following 2 conditions for the D_4^{12} caustic.

$$\begin{aligned} M_{11}(q) &= M_{22}(q)\,, \\ M_{12}(q) &= 0\,. \end{aligned} \tag{4.25}$$

These two conditions immediately imply that the matrix $\tilde{\mathcal{M}}$ is proportional to the identity matrix,

$$\tilde{\mathcal{M}} = \begin{pmatrix} \mu & 0 \\ 0 & \mu \end{pmatrix}. \tag{4.26}$$

D_4 singularities and A_3 varieties

An additional important consequence of the inferred constraints 4.25 for the D_4 singularities is that D_4^{ij} points will always be located on the two corresponding A_3 varieties,

A_3^i and A_3^j. We may infer this from the following observation. In the coordinate system introduced above (cf. eq. 4.18), the eigenvector for the third eigenvalue μ_3 is given by $v_3 = (0, 0, 1)$. The eigenvectors v_1 and v_2 both lie in the q_1q_2-plane, and since the matrix $\tilde{\mathcal{M}}$ is degenerate we have the freedom to take them to be orthogonal to the gradient of the corresponding eigenvalue fields. This means that

$$\begin{aligned} v_1 \cdot \nabla\mu_1 &= \mu_{1,1} = 0\,, \\ v_2 \cdot \nabla\mu_2 &= \mu_{2,2} = 0. \end{aligned} \tag{4.27}$$

This proves the unfolding $D_4^{ij} \to A_3^i$ and $D_4^{ij} \to A_3^j$. For the relations between the singularity classes see section 6.1. For a formal proof see Hidding *et al.* (2014).

The D_4 location

Shell-crossing for A caustics is a one-dimensional process. A direct implication of this is that the related critical points are equivalent up to diffeomorphisms. For the D family this is no longer true. Shell-crossing for the D-family is two dimensional. As a consequence, the D_4 class consist of hyperbolic (D_4^+) and elliptic (D_4^-) umbilic points, i.e.

$$D_4^{ij}(t) = D_4^{+ij}(t) \cup D_4^{-ij}(t)\,. \tag{4.28}$$

In order to infer the corresponding caustic conditions we consider the two constraint quantities $Q_1(q)$ and $Q_2(q)$ (see eq. 4.25),

$$\begin{aligned} Q_1(q) &= \frac{M_{11}(q) - M_{22}(q)}{2}\,, \\ Q_2(q) &= M_{12}(q)\,, \end{aligned} \tag{4.29}$$

which at the D_4 singularity location vanish, i.e. $Q_1(D_4) = 0$ and $Q_2(D_4) = 0$. By a Taylor expansion of $Q_1(q)$ and $Q_2(q)$ in a neighbourhood around the D_4 singularity, we find that for points located in the q_1q_2-plane,

$$\begin{aligned} Q_1(q) &= a\,q_1 + b\,q_2\,, \\ Q_2(q) &= c\,q_1 + d\,q_2\,. \end{aligned} \tag{4.30}$$

In this expansion, we have taken the D_4 singularity to define the origin of the coordinate system. In this expansion, the parameters a, b, c and d are the derivatives of $Q_1(q)$ and $Q_2(q)$ at the D_4 location,

$$a = \frac{1}{2}\frac{\partial(M_{11} - M_{22})}{\partial q_1},\ b = \frac{1}{2}\frac{\partial(M_{11} - M_{22})}{\partial q_2},\ c = \frac{\partial M_{12}}{\partial q_1},\ d = \frac{\partial M_{12}}{\partial q_2}\,. \tag{4.31}$$

As proposed by Delmarcelle (1995), the determinant $S_{\mathcal{M}}$ of the corresponding Q_1Q_2 map,

$$S_{\mathcal{M}} = bc - ad = \frac{1}{2}\left[(M_{112} - M_{222})M_{112} - (M_{111} - M_{122})M_{122}\right]\,, \tag{4.32}$$

is invariant under rotations in the q_1q_2-plane †. In the expression above, we have used the expressions

$$M_{iik} = \frac{\partial M_{ii}}{\partial q_k}\,, \quad M_{ikk} = \frac{\partial M_{ik}}{\partial q_k}\,. \tag{4.33}$$

Using the relations between the matrix elements M_{11}, M_{22} and M_{12} and the eigenvalues

† In fact, it can be shown that this determinant is a third-order invariant under rotations (Delmarcelle 1995).

μ_1 and μ_2, we may recast the determinant $S_{\mathcal{M}}$ in an explicit expression incorporating these eigenvalues,

$$S_{\mathcal{M}} \;=\; \frac{1}{2}\left[(\mu_1-\mu_2)_{,2}\mu_{1,2} - (\mu_1-\mu_2)_{,1}\mu_{2,1}\right]. \tag{4.34}$$

As Delmarcelle (1995) pointed out, the transformation can be shown to consist of two branches. Their identification surfaces via a rescaling of the determinant via the multiplication by a *positive* number. We then find that the two branches correspond to two separate singularity classes of the D_4 family,

$$D_4^{\pm ij}(t) = \{q \in L | q \in A_2^i(t) \cap A_2^j(t) \wedge \mathrm{sign}(S_{\mathcal{M}}) = \pm 1\}, \tag{4.35}$$

where the points $q \in A_2^i(t) \cap A_2^j(t)$ are the points for whom at time t the caustic conditions are simultaneously valid for two eigenvalues, i.e. $1+\mu_i = 1+\mu_j = 0$. Integrated over time, these $D_4^{\pm ij}(t)$ points trace out the curves $D_4^{\pm ij}$,

$$D_4^{\pm ij} \;=\; \{q \in L | q \in A_2^i(t) \cap A_2^j(t) \wedge \mathrm{sign}(S_{\mathcal{M}}) = \pm 1, \text{ for some time } t\}. \tag{4.36}$$

4.2.2. *The $D_4^{\pm}$ points*

The topology of the $D_4^{\pm ij}(t)$ variety changes at $D_4^{\pm}$ and D_5 points.

The $D_4^{\pm}$ points are analogous to the $A_4^{\pm}$ points of the A-family. The $D_4^{\pm}$ points occur when ith and jth eigenvalue field, μ_i and μ_j, restricted to the points q in the $D_4^{\pm ij}$ variety reaches a minimum or maximum, i.e.

$$\begin{aligned} D_4^{ij+} \;&=\; \{q \in L | q \in D_4^{+ij}(t) \;\wedge\; \mu_{tk}(q) \text{ max-/min. of } \mu_{tk}|_{D_4^{+ij}} (k = i \text{ or } k = j) \text{ for some } t\} \\ D_4^{ij-} \;&=\; \{q \in L | q \in D_4^{-ij}(t) \;\wedge\; \mu_{tk}(q) \text{ max-/min. of } \mu_{tk}|_{D_4^{-ij}} (k = i \text{ or } k = j) \text{ for some } t\} \end{aligned} \tag{4.37}$$

Particularly interesting is the fact that the $D_4^{\pm}$ points are always created as a pair. Two D_4^{+} points are created simultaneously, as are D_4^{-} points. By implication, also the $D_4^{\pm}$ curves (eq. 4.36) are always created in pairs. This is in contrast to the D_5 points, which go along with the creation of a pair consisting of a D_4^{+} and a D_4^{-} point.

4.2.3. *The D_5 caustics*

The shell-crossing condition applied to the D_4^{ij} variety yields the caustic conditions for the D_5 parabolic umbilic singularity.

The manifold D_4^{ij} forms a singularity in the point $q_s \in D_4^{ij}(t)$ if and only if the tangent vector $T \in T_{q_s} D_4^{ij}$ is normal to v_k, with $k \neq i, j$. Hence, the normal, $n = \nabla(\mu_{ti} - \mu_{tj})$, is orthogonal to both v_i and v_j,

$$\begin{aligned} (\mu_i - \mu_j)_{,i} \equiv v_i \cdot \nabla(\mu_{ti} - \mu_{tj}) \;&=\; 0, \\ (\mu_i - \mu_j)_{,j} \equiv v_j \cdot \nabla(\mu_{ti} - \mu_{tj}) \;&=\; 0. \end{aligned} \tag{4.38}$$

The collection of all such points

$$D_5^{ij} = \{q \in L | q \in D_4^{ij}(t) \quad \wedge \quad (\mu_i - \mu_j)_{,i} = (\mu_i - \mu_j)_{,j} = 0 \quad \text{for some time } t\}, \tag{4.39}$$

The elliptic and hyperbolic umbilic ($D_4^{\pm}$) points merge in parabolic umbilic (D_5) points, since $D_5^{ij}(t) \subset D_4^{ij}(t)$ and

$$S_{\mathcal{M}} = \frac{1}{2}\left\{(\mu_i - \mu_j)_{,j}\mu_{i,j} - (\mu_i - \mu_j)_{,i}\mu_{j,i}\right\} \;=\; 0. \tag{4.40}$$

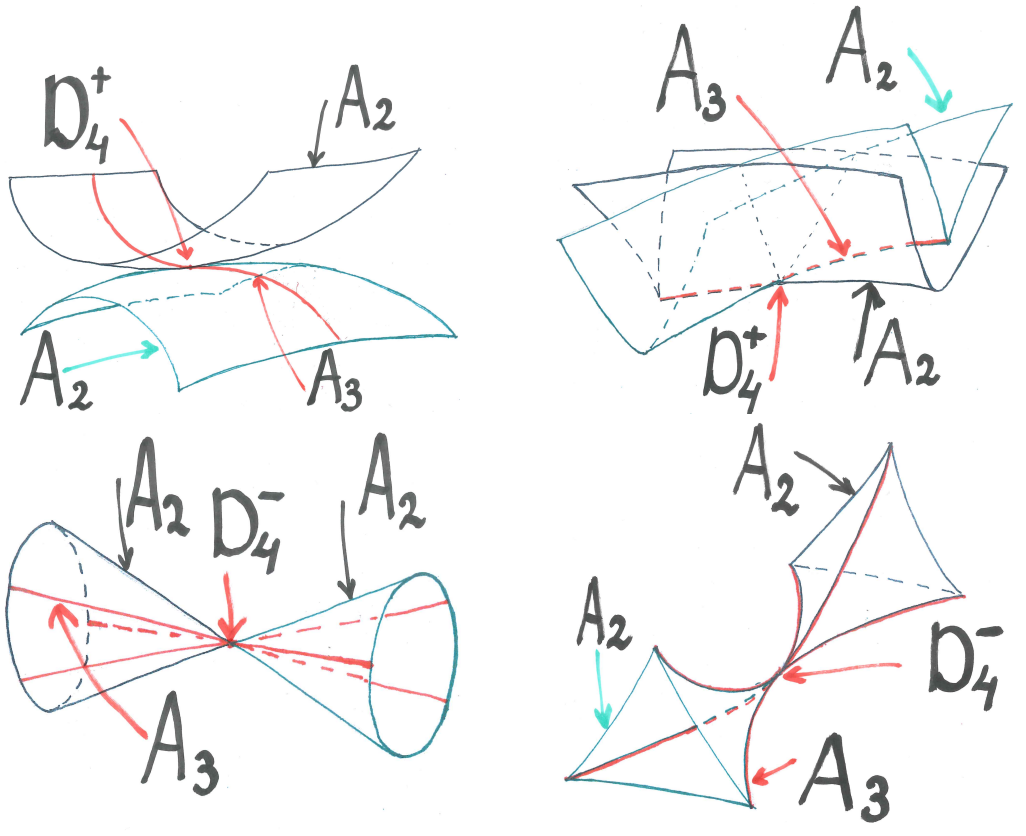

Figure 12: The hyperbolic/elliptic umbilic ($D_4^{\pm}$) singularities. The upper two panels show the elliptic umbilic (D_4^{+}) singularity. The lower panels show the hyperbolic umbilic (D_4^{-}) singularity. The two panels on the left are their representations in Lagrangian space and the two panels on the right their representation in Eulerian space. The black sheets are fold (A_2) sheets corresponding to one eigenvalue field. The green sheets are fold (A_2) sheets corresponding to a second eigenvalue field. The red lines are cusp (A_3) curves. The point in the center depict the hyperbolic/elliptic umbilic ($D_4^{\pm}$) singularities. The hyperbolic umbilic (D_4^{+}) and elliptic umbilic (D_4^{-}) singularity are also known as the purse and pyramid singularity.

The D_5 points are stable singularities in the classification of Lagrangian singularities. For general dynamics they are unstable and not included in the classification scheme.

4.3. *the Caustic Skeleton & the Cosmic Web*

The process of formation and evolution of structure in the Universe is driven by the gravitational growth of tiny primordial density and velocity perturbations. When it reaches a stage at which the matter distribution starts to develop nonlinearities, we see the the emergence of complex structural patterns. In the current universe we see this happening at Megaparsec scales. On these scales, cosmic structure displays a marked intricate weblike pattern, the Cosmic Web. Prominent elongated filamentary features define a pervasive network. Forming the dense boundaries around large tenuous sheetlike

membranes, the filaments connect up at massive, compact clusters located at the nodes of the network and surround vast, underdense and near-empty voids.

The gravitational structure formation process is marked by vast migration streams, known as cosmic flows. Inhomogeneities in the gravitational force field lead to the displacement of mass out of the lower density areas towards higher density regions. Complex structures arise at the locations where different mass streams meet up. Gravitational collapse sets in as this happens. In terms of six-dimensional phase space, it corresponds to the local folding of the phase space sheet along which matter – in particular the gravitationally dominant dark matter component – has distributed itself.

The positions where streams of the dark matter fluid cross are the sites where gravitational collapse occurs. The various types of caustics described and classified in our study mark the different configurations in which this process may take place. Their locations trace out a Lagrangian skeleton of the emerging cosmic web, marking key structural elements and establishing their connectivity (also see the discussion in Hidding *et al.* (2014)). In other words, the A_3, A_4, A_5, D_4, D_5 varieties, in combination with the corresponding $A_3^{\pm}, A_4^{\pm}$, and $D_4^{\pm}$ points, are the dynamical elements whose connectivity defines the weaving of the the cosmic web (Zel'dovich 1970; Bond *et al.* 1996; van de Weygaert & Bond 2008; Aragón-Calvo *et al.* 2010*b*; Cautun *et al.* 2014).

On the basis of this observation, we may obtain the skeleton of the cosmic web in Eulerian space by means of the Lagrangian map x_t to Eulerian space. Following the identification of the various caustic varieties and caustic points in Lagrangian space, the application of the map x_t will produce the corresponding weblike structure in Eulerian space. A telling example of the resulting patterns and their comparison with a fully nonlinear N-body simulation of the corresponding evolving matter distribution is shown in figure 13.

The three panels in the lefthand column of figure 13 show the Lagrangian skeleton for a two-dimensional fluid. The fluid is taken to evolve according to the Zel'dovich approximation (Zel'dovich (1970), see appendix A), which represents a surprisingly accurate first-order Lagrangian approximation of a gravitationally evolving matter distribution (see e.g. Shandarin & Zel'dovich 1989). The initial density field of the displayed models is that of a Gaussian random density field (see Adler 1981; Bardeen *et al.* 1986), which according to the latest observations and to current theoretical understanding is an accurate description of the observed primordial matter distribution (see e.g. Planck Collaboration *et al.* 2016; Komatsu *et al.* 2003; Creminelli *et al.* 2006).

To enable our understanding of the hierarchical process of structure formation and the resulting multiscale structure of the cosmic web, we assess the caustic structure of the Lagrangian matter field at three different resolutions. In figure 13 the field resolution decreases from the top panels to the bottom panels, as the initial density field was smoothed by an increasingly large Gaussian filter. The contour maps that form the background in these panels represent the resulting initial density fields. The red lines trace the A_3 variety, i.e. the A_3 lines, for the largest eigenvalue μ_1 field (also see fig. 3 to appreciate how they are related). Also the $A_3^{\pm}$ points and $D_4^{\pm}$ points are shown, the first as red dots, the latter as black triangles.

The resulting weblike structure in Eulerian space is depicted in the corresponding righthand panels. The A_3 lines, $A_3^{\pm}$ points and $D_4^{\pm}$ points are mapped to their Eulerian location by means of the Zel'dovich approximation. The red lines, red dots and black triangles represent the Eulerian skeleton corresponding to the Zel'dovich approximation. These are superimposed on the density field of the corresponding N-body simulations. The comparison between the latter and the Eulerian skeleton reveal that the caustic skeleton – the assembly of A_3 lines, $A_3^{\pm}$ points and $D_4^{\pm}$ points – trace the principal

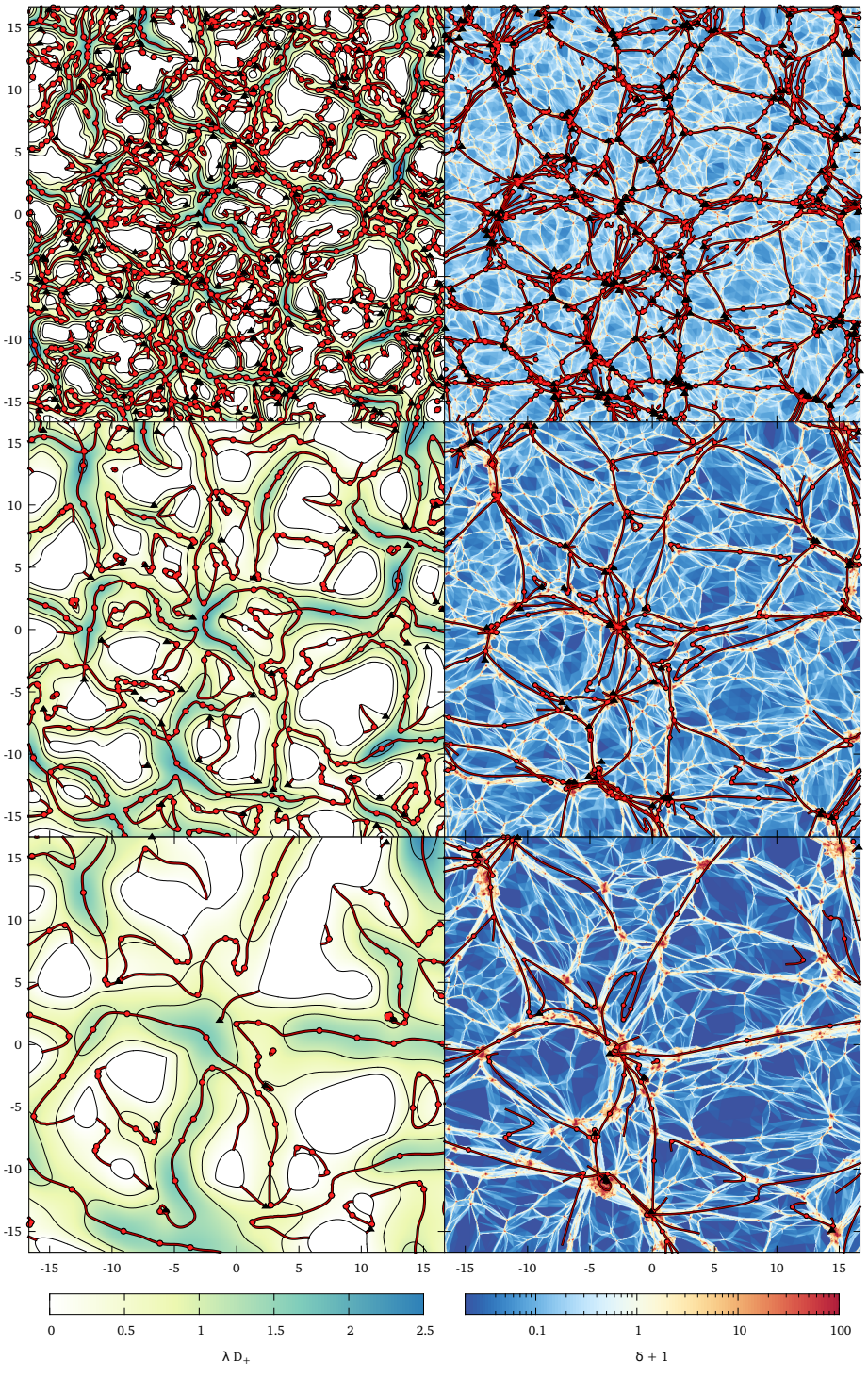

Figure 13: Spatial distribution of singularities in the Lagrangian and Eulerian Cosmic Web. The figure compares the spine of the cosmic web with the mass distribution in a 2-D N-body simulation. Left panel: initial field of density fluctuations and the skeleton of identified singularities/catastrophes. Right panel: density field of an evolved 2D cosmological N-body simulation, in which the Lagrangian skeleton of singularities is mapped by means of the Zel'dovich approximation. From Feldbrugge (2014).

elements and connections of the cosmic web seen in the N-body simulations remarkably well. Moreover, by assessing the caustic structure at different resolutions of the density field, one obtains considerable insight into the multiscale structure and topology of the cosmic web.

The ability to relate the caustic skeleton to the statistical nature of the primordial density field makes it possible to use the structure of the current cosmic web to the nature of the Gaussian initial density field, and hence of the underlying cosmology. It means that our analysis of the caustic skeleton may define a rich foundation for exploiting the structure of the observed cosmic web towards constraining global cosmological parameters and the cosmic structure formation process. For such a statistical treatment of 2-dimensional fluids, we refer to Feldbrugge *et al.* (2014). A more extensive analysis of the statistics of 2- and 3-dimensional caustic skeleton will follow in Feldbrugge *et al.* (2017).

5. Classification of singularities

The form and morphology in which the various singularities that were inventorized in the previous section will appear in the reality of a physical system depends on several aspects. The principal influence concern the dynamics of the system, as well as its dimensionality. The dynamics determines the way the fluid evolves, to a large extent via its dominant influence on the accompanying flow of the fluid. This affects the morphology of the fluid, and in particular the occurrence of singularities. Evidently, also the dimensionality of the fluid process will bear strongly on the occurrence and appearance of singularities. Higher spatial dimensions may enlarge the number of ways in which a singularity may form. It also influences the ways in which singularities can dynamically transform into one another.

In this section, we seek to provide an impression of the possible variety in appearance of singularities. To this end, we will first discuss the generic singularity classification scheme that we follow. It is not the intention of this study to provide an extensive listing of all possible classes of fluids. Instead, to make clear in how different physical situations may affect the appearance of singularities, we restrict our presentation of classification schemes to two different classes of fluids. We also restrict our inventory to fluids in a three dimensional context. It is the most representative situation, and at the same time offers a good illustration of other configurations.

5.1. *Classes of Lagrangian fluids*

To appreciate the role of the dynamics in constraining the evolution and appearance of a fluid, and that of the formation and fate of the singularities in the fluid, it is important to understand and describe its evolution in terms of six-dimensional phase space.

One way of defining phase space $\mathcal{C}$ is in terms of the Cartesian product of Lagrangian and Eulerian manifolds L and E, i.e. $\mathcal{C} = L \times E$. In this context, the phase space coordinates of a mass element are (q, x). Every point in phase space $(q, x) \in \mathcal{C}$ represents the initial and final position q and x of a mass element at some time t. Evidently, one may also opt for the more conventional definition consisting of space coordinates x and canonical momenta p, in which case the phase space coordinate of a mass element are given by (x, p). However, for the description of Lagrangian fluid dynamics it is more convenient to follow the first convention. We should note that for this description of phase space Liouville's theorem does not apply, specifically not for the Euclidean notion of volumes.

At the initial time $t = 0$, the Lagrangian map is the identity map, i.e. for all $q \in L$ $x_0(q) = q$. In phase space $\mathcal{C}$, the fluid then occupies the submanifold $\mathcal{L}_0 = \{(q, x_0(q)) \in \mathcal{C} | q \in L\}$. If we equip $\mathcal{C}$ with a symplectic structure ω, we can prove this to be a so-called Lagrangian submanifold (for a precise definition of Lagrangian submanifolds see appendix B).

Differences in the dynamics of a fluid reveal themselves in particular through major differences in the phase space structure and topology of the manifolds delineated by the mass elements. To provide an impression of the differences in morphology and classification of singularities emerging in fluids of a different nature, specifically that of fluids with a different dynamical behaviour, we concentrate the discussion on two different classes of Lagrangian fluids:

(i) *Generic Lagrangian fluids.*
Lagrangian fluids for which the map $x_t : L \to E$ is a generic continuous and differentiable mapping from L to E for every time t. The dynamics does not restrict the map x to any extent. We describe the classification up to local diffeomorphisms, i.e. two singularities are considered equivalent if and only if there exist local coordinate transformations, which map them into each other.

(ii) *Lagrangian fluids with Hamiltonian dynamics.*
The evolution of the fluid is governed by a Hamiltonian. This assumption restricts the possible evolution of the fluid. Formally, the map x corresponds uniquely to a so-called Lagrangian map. The singularities of Lagrangian maps, known as Lagrangian singularities, are classified up to Lagrange equivalence.

Lagrangian fluids with Hamiltonian dynamics form an important class of fluids: fundamental theories of particle physics generally allow for a Hamiltonian description. Nonetheless, in a range of practical circumstances we may encounter fluids that are either more or less constrained. An example are fluids with effective dynamics. They contain friction terms which are not described by Hamiltonian systems. Such fluid systems are less restrictive than those that are specifically Hamiltonian. On the other hand, there are also Hamiltonian fluids that are characterized by additional constraints.

Systems that are characterized by either more or less constraints may involve different classification schemes than regular Hamiltonian fluids. While it is beyond the scope of this study to provide a complete, and exhaustive, inventory of all classification scheme, the comparison between the classification schemes of two different fluid configurations will provide an impression of the variety. The principal intention is to provide an understanding of the robustness of Hamiltonian systems.

5.2. *Singularity Classification*

As we observed at the beginning of this paper (see eqn. 2.4), singularities form when the deformation tensor $\mathcal{M}$ of the Lagrangian map $x_t : L \to E$, from Lagrangian space L to Eulerian space E, is non-invertible. In such situations, one or more of the eigenvalues μ_i have $\mu_i + 1 = 0$. The emerging singularities can be classified into several families. Here we follow the classification scheme defined by Bruce (1985) for singularities of generic one-family maps $x(q) : L \to E$.

For practical reasons, we restrict the presentation of the classification to the case of L and E being three-dimensional spaces. We also restrict ourselves to the classification of stable singularities. Stability in this sense means that the singularities do not change in character when a small fluctuation is applied to the Lagrangian map. It means that

if the map x_t has a stable singularity in point p at time t, then the map $x_t + \delta x_t$ with δx_t sufficiently small, has a singularity in the same equivalence class at a point close to p at a time close to t. Because in practical situations unstable singularities only have a probability measure zero to occure, we will not include them in our consideration.

For the situation of three-dimensional fluids, we may use the formal criterion of their corank to split the equivalence classes of singularities into three groups. The corank of a matrix is defined as the number of spatial dimensions minus the rank of the matrix. It leads to the following scheme, in which we recognize the singularities identified in the previous sections,

---

A_k class.
When the deformation tensor $\mathcal{M}$ is non-invertible due to one eigenvalue, it has corank 1. These singularities are classified by the A_k classes.

D_k class.
When $\mathcal{M}$ is non-invertible due to two eigenvalues, the singularity has co-rank 2. Singularities with co-rank 2 are classified as D_k classes.

E_k class.
In 3-dimensional fluids, the points for which the Hessian has co-rank 3 is of measure zero. Following this observation, we do not consider these E_k class singularities.

Given that the E_k singularities in practice will never occur, we will restrict the discussion of the singularity classification scheme to the A_k and D_k classes.

5.3. *Singularity Classification: generic fluids*

For the classification of singularities of generic one-family maps $x : L \to E$, with L and E three-dimensional, we follow the classification by Bruce (1985). Important for our purpose, is that it can be shown that the singularities that may emerge in generic mappings from $L \to E$ are equivalent to those emerging in the simple linear maps

$$x_t(q) = q + t\, u(q)\,, \tag{5.1}$$

in which u is a vector field on L. In general, the vector field $u(q)$ contains both a longitudinal and a transversal part,

$$u(q) \;=\; u_l(q) + u_t(q)\,. \tag{5.2}$$

The longitudinal component corresponds to potential motion and has curl zero, $\nabla \times u_l = 0$, while the transversal component has divergence zero, $\nabla \cdot u_t = 0$. When the motion is restricted to its longitudinal component, the displacement $s_t(q)$ effectively is that of ballistic motion.

The classification of singularities in general Lagrangian fluid dynamics is expressed by theorem 3. We restrict ourselves to listing the classification scheme of Bruce (1985), in terms of the generic expressions for the maps $x_t(q)$ of each of the classified singularities. The maps $x_t(q)$ in the corresponding table assume that the singularity occurs at the origin $q = 0$, at $t = 1$. In appendix C we show that these normal forms indeed satisfy

the corresponding caustic conditions. For the proofs and in-depth derivations we refer to Bruce (1985).

THEOREM: 3.
A stable singularity occurring in a Lagrangian fluid with generic dynamics is, up to local diffeomorphisms, equivalent to one of the following classes:

Singularity class	*Map* $x_t(q)$	*Singularity name*
A_1	$x_t(q) = q$	*trivial case*
A_2	$x_t(q) = q + t\left(0, 0, q_3^2 - q_3\right)$	*fold*
A_3	$x_t(q) = q + t\left(0, 0, q_1 q_3 + q_3^3 - q_3\right)$	*cusp*
A_4	$x_t(q) = q + t\left(0, 0, q_1 q_3 + q_3^4 - q_3\right)$	*swallowtail*
A_5	$x_t(q) = q + t\left(0, 0, q_1 q_3 + q_2 q_3^2 + q_3^5 - q_3\right)$	*butterfly*
$D_4^{\pm}$	$x_t(q) = q + t\left(0, q_2 q_3 - q_2, q_2^2 \pm q_3^2 + q_1 q_2 - q_3\right)$	*hyperbolic/elliptic*
$A_3^{\pm}$	$x_t(q) = q + t\left(0, 0, (q1^2 \pm q_2^2) q_3 + q_3^3 - q_3\right)$	
$A_4^{\pm}$	$x_t(q) = q + t\left(0, 0, q_1 q_3 \pm q_2^2 q_3^2 + q_3^4 - q_3\right)$	

Note: The expressions in the table assume that the singularity occurs at the origin $q = 0$*, at* $t = 1$*. The first five singularity classes are the A-family. The subsequent class is the D-family. The last two are the normal forms of the* A_3 *and* A_4 *points. The* A_k *class has co-rank* 1 *and co-dimension* $k-2$*. The* $D_4^{\pm}$ *singularities have co-rank* 2 *and are one-dimensional (Bruce 1985).*

5.4. *Singularity Classification: Hamiltonian fluids*

The evolution of Lagrangian fluids with Hamiltonian dynamics is more constrained than that of generic Lagrangian fluids. As the fluid develops complex multistream regions, the phase space submanifold $\mathcal{L}_t = \{(q, x_t(q)) | q \in L\}$ for fluids with Hamiltonian dynamics remains Lagrangian. For generic fluid dynamics this is no longer true.

A key step in evaluating the emerging singularities is that of connecting the displacement map $x_t(q)$ to the Lagrangian map. In appendix B.2, we describe in some detail how a given Lagrangian map can be constructed from a Lagrangian submanifold $\mathcal{L}$. A Lagrangian map can develop regions in which multiple points in the Lagrangian manifold are mapped to the same point in the base space.

Lagrangian singularities are those points at which the number of pre-images of the Lagrangian map undergoes a change. Lagrangian catastrophe theory (Arnol'd (1972); Arnol'd *et al.* (2012*b*)) classifies the stable singularities. This refers to the stability of singularities with respect to small deformations of the Lagrangian manifold of $\mathcal{L}$. This is true up to Lagrangian equivalence, a concept that is a generalization of equivalence up to coordinate transformation. For a more formal and precise definition of Lagrangian equivalence see appendix B.

It can be demonstrated (see Arnol'd *et al.* 2012*b*) that every Lagrangian map $l : \mathcal{L} \to \mathcal{C} \to E$ is locally Lagrangian equivalent to a so-called gradient map. In other words, it means the corresponding map x_t is locally equivalent to

$$x_t(q) = \nabla_q S_t \,, \tag{5.3}$$

in which $S_t : L \to \mathbb{R}$, for all q and t, is a scalar function. By recasting S_t in terms of a function $\Psi_t : L \to \mathbb{R}$,

$$S_t = \frac{1}{2}q^2 + \Psi_t(q)\,, \tag{5.4}$$

we find that locally the map x can be written in the form

$$x_t(q) = q + \nabla_q \Psi_t(q)\,. \tag{5.5}$$

Evidently, this implies that the displacement map is longitudinal, and that the corresponding Jacobian $\partial s_t/\partial q$ is symmetric.

The classification of singularities of a Lagrangian fluid with Hamiltonian dynamics is expressed by theorem 4. The classification scheme listed is that of Bruce (1985). Also here, the maps $x_t(q)$ in the table are for the singularity located at the origin $q = 0$, at $t = 1$. In appendix C it is shown that these normal forms indeed satisfy the corresponding caustic conditions. For proofs we refer to Bruce (1985).

THEOREM: 4.
A stable Lagrangian singularity of a Lagrangian fluid with Hamiltonian dynamics, is locally Lagrange equivalent to one of the following classes:

Singularity class	*Map* $x_t(q)$	*Singularity name*
A_1	$x_t(q) = q$	*trivial case*
A_2	$x_t(q) = q + t\left(0, 0, q_3^2 - q_3\right)$	*fold*
A_3	$x_t(q) = q + t\left(\frac{1}{2}q_3^2, 0, q_3(q_1 - 1)\right)$	*cusp*
A_4	$x_t(q) = q + t\left(\frac{1}{2}q_3^2, 0, q_1 q_3 + q_3^4 - q_3\right)$	*swallowtail*
A_5	$x_t(q) = q + t\left(\frac{1}{2}q_3^2, \frac{1}{3}q_3^3, q_1 q_3 + q_2 q_3^2 + q_3^5 - q_3\right)$	*butterfly*
$D_4^{\pm}$	$x_t(q) = q + t\big(\pm q_1 q_2 - q_1,$ $\pm\left(\frac{1}{2}q_1^2 + \frac{3}{2}q_2^2\right) + 2q_2 q_3 + 2q_2^3 - q_2, q_2^2\big)$	*hyperbolic/elliptic*
D_5	$x_t(q) = q + t\left(0, q_2^3 - q_2, q_3^3 - q_3\right)$	*parabolic*
$A_3^{\pm}$	$x_t(q) = q + t\left(q_1 q_3^2, \pm q_2 q_3^2, (q1^2 \pm q_2^2)q_3 + q_3^3 - q_3\right)$	
$A_4^{\pm}$	$x_t(q) = q + t\left(\frac{1}{2}q_3^2, \pm\frac{2}{3}q_2 q_3^3, q_1 q_3 \pm q_2^2 q_3^2 + q_3^4 - q_3\right)$	

Note: The expressions in the table assume that the singularity occurs at the origin $q = 0$*, at* $t = 1$*. The first five singularity classes are the A-family. The subsequent two are the D-family. The last two are the normal forms of the* A_3 *and* A_4 *points. The* A_k *class has co-rank* 1 *and co-dimension* $k - 2$*. The* D_k *singularities have co-rank* 2 *and co-dimension* $k - 2$ *(Arnol'd 1972).*

Comparing the classification schemes for generic Lagrangian singularities and those for Lagrangian fluids with Hamiltonian dynamics, we may note the similarities in the classification. Both classifications have an A and a D family. It can be demonstrated that the A singularity classes of the scheme for Lagrangian fluids with Hamiltonian dynamics are contained in those corresponding to the generic Lagrangian fluid. Concretely, this means that a displacement field corresponding to the Hamiltonian A_k class is also an element of the generic A_k class. On the other hand, there are significant differences in the case of the D families.

The D families are some what different. The Hamiltonian D_4 class is contained in the generic D_4 class. However, the Hamiltonian D_5 class has no analogue in the generic classification scheme. This is a result of the D_5 singularity not being stable under coordinate transformations.

A final remark concerns the singularity classification schemes for higher dimensional fluids. For these a more elaborate classification scheme applies. This classification scheme is described in appendix B.

5.5. *Unfoldings*

Singularities generally change their class upon small, but finite, deformations of the displacement map s_t. The corresponding evolution of a singularity follows the universal unfolding process of singularities. The general behavior is described in the following unfolding diagram, in which the arrows indicate the singularity into which specific singularities can transform.

$$\begin{array}{ccccccccc} A_1 & \leftarrow & A_2 & \leftarrow & A_3 & \leftarrow & A_4 & \leftarrow & A_5 \\ & & & & & \nwarrow & & \nwarrow & \\ & & & & & & D_4 & \leftarrow & D_5 \end{array}$$

For $i \geqslant 2$, the A_i singularities decay into A_{i-1} singularities. For $i \geqslant 5$, the D_i singularities decay into either A_{i-1} or D_{i-1} singularities. In section 6 we will describe how the decay of singularities is connected to the evolution of the large-scale structure in the Universe and in outlining the spine of the cosmic web.

5.6. *Density profile*

Vasil'ev (1978) inferred the density profiles of the various classes of singularities, in case they emerrge as a result of potential motion in a collision-less self-gravitating medium. For each of the mass concentrations in and around these singularities, he found scalefree power-law profiles. The radially average profiles display the following decrease of density $\rho(r)$ as a function of radius r.

Singularity class	Singularity name	Profile $\rho(r)$
A_2	fold	$\rho(r) \propto r^{-1/2}$
A_3	cusp	$\rho(r) \propto r^{-2/3}$
A_4	swallowtail	$\rho(r) \propto r^{-3/4}$
A_5	butterfly	$\rho(r) \propto r^{-4/5}$
D_4	hyperbolic/elliptic	$\rho(r) \propto r^{-1}$
D_5	parabolic	$\rho(r) \propto r^{-1} \log(1/r)$

With respect to these radially averaged profiles, we should realize that the mass distribution in and around the singularities is highly anisotropic. This is true for any dimension in which we consider the structure around the singularities.

Notwithstanding this, we do observe that the steepest density profiles are those around the point singularities A_5 and D_5. However, they are mere transient features that will only exist for a single moment in time. The point singularities A_4 and D_4 display a less pronounced behaviour. However, they move over time. Also, we see that the cusp

singularity A_3 possesses a steeper mass distribution that that in and around the sheet singularity A_2.

6. Dynamics of caustics

The caustic conditions presented and extensively discussed in this study reveal the profound relationship between the various classes of singularities that may surface in fluids. Indeed, dependent on the dynamics of the system as the fluid evolves it may start to develop pronounced structures. As this happens, we may observe the emergence of the first singularities. As its dynamical evolution proceeds to more advanced stages, we not only see the appearance of more singularities, but also the transformation of one class of singularities into another one. Changes in the local geometry may also reflect the merging of singularities into a new singularity, in itself a manifestation of a hierarchical buildup of structural complexity.

When we follow the evolution of a fluid, we start at a an initial time $t = 0$. At that time, the displacement map s_t is the zero map. Amongst others, this implies the fluid does not (yet) contain singularities. As the fluid evolves, the phase space sheet that it occupies in six-dimensional space gets increasingly folded. Its projection on Euclidian space follows this process. It is here that we see that the fluid develops singularities as a result of the folding process. To facilitate and guide our visual intuition for the iterative folding of singularities in phase space that we describe below, we refer to figure 3.

The principal family of singularities - principal in terms of rate of occurrence and spatial dominance - is the A-family. They are induced by singularities in the geometric structure of one of the eigenvalue fields. In physical terms, they involve one-dimensional collapse on to the emerging singularity.

The most prominent and abundant singularities are those of the two-dimensional fold sheets $A_2^i(t)$. In Eulerian space, they mark the regions where mass elements are turned inside out as the Lagrangian density attains infinity. This happens while they represent the locations where separate matter streams are crossing each other. As time proceeds, the fold sheets $A_2^i(t)$ sweeping over an increasingly larger Lagrangian region. Ultimately, integrating over time, they mark an entire Lagrangian volume, which is labelled as A_2^i. The A_2^i set form a three-dimensional variety.

When we wish to identify where a particular individual fold sheet is born, we turn to the cusp points A_3^{i+}. They are the points on the fold sheets where the corresponding eigenvalue field attains an extremum. Because of this, they mark the sites of birth of the fold singularities. As the $A_2^i(t)$ sheets unfold, at the edges their surface gets wrapped in a higher order singularity, the cusp curves $A_3^i(t)$. In time, these curves move through space and trace out cusp sheets A_3^i. When e.g. looking at the Megaparsec scale matter distribution in the Universe, the cusp sheets are to be associated with a key element, the walls or membranes in the cosmic web.

A dynamically interesting process occurs at the the cusp points A_3^{i-}, which are the saddle points of the corresponding eigenvalue field μ_{ti} that at a given time are encapsulated by the fold sheet A_2^i. At the A_3^{i-} points, we see the merging or annihilation of fold sheets A_2^i into a larger structure. Mathematically, they mark the key locations where the topology of the eigenvalue field changes abruptly. Physically, they are associated with the merging of separate structural components, a manifestation of the hierarchical buildup of structural complexity.

Also the cusp curves $A_3^i(t)$ can get folded. In Eulerian space, the folding of the cusp curves manifests itself as $A_4^i(t)$ swallowtail points. As time proceeds, these points move

through space and define the swallowtail curve A_4^i. It is of interest to note that the swallowtail curve is embedded in the cusp sheet, i.e. $A_4^i \subset A_3^i$. In the context of cosmic structure formation the swallowtail curves outline and trace perhaps the most outstanding feature of the cosmic web, the pronounced elongated filaments that form the of spine the weblike network (cf. eg. Aragón-Calvo *et al.* (2010*a*)). Also these features build up in a hierarchical process of small filaments merging into ever larger and more prominent arteries. In the context of the evolving singularity structure that we study, this process is represented by the A_4^{i+} points and A_4^{i-} points. They define the decisive junctions where significant changes in topology occur. For the $A_4^{i\pm}$ points this concerns their identity in the gradient of the eigenvalue field, in which the A_4^{i+} are maxima and minima and A_4^{i-} points are the saddle points. The implication of this is that cusp curves get created or annihilated at A_4^{i+} points, while they merge or separate at A_4^{i-} points.

The final morphological constituent in this structural hierarchy of singularities is that of the butterfly points A_5^i. They conclude the A-family of singularities, i.e. the family of singularities that correspond to the spatial characteristics of the field of one eigenvalue μ_i. The swallowtail curves A_4^i get folded at A_5^i butterfly points. In the three-dimensional structural pattern that formed in the fluid, these will represent nodes. In the cosmic web, they define the nodal junctions, connecting to the various filamentary extensions that outline its spine. In principle, for a given initial field and dynamical evolution, one might use these identifications to eg. evaluate how many filaments are connected to the network nodes (see e.g. Aragón-Calvo *et al.* (2010*b*)).

Of a more challenging nature within the evolutionary unfolding of the patterns emering in fluid flow is the formation of the D family of singularities. They occur when two fold sheets corresponding to different eigenvalue fields intersect. By implication, this means that the D singularities connect A singularities corresponding to two eigenvalue fields.

The $A_2^i(t)$ and $A_2^j(t)$ sheets, with $i \neq j$, intersect in the elliptic and hyperbolic umbilic points $D_4^{\pm ij}(t)$. In contrast to the A family of singularities, the collapse into D singularities is two-dimensional. It leads to the birth of the socalled *umbilic* points. Over time, they trace out the umbilic curve $D_4^{\pm ij}$. The collapse process may occur in two distinctive ways, indicated by the labels $+$ and $-$.

The topology of the variety $D_4^{\pm ij}(t)$ changes at $D_4^{ij\pm}$ and D_5 points. An interesting characteristic of umbilic curves is that they are always created or annihilated in pairs. The $D_4^{ij\pm}$ points correspond to the creation or annihilation of two $D_4^{\pm ij}$ curves of the same signature. By contrast, the D_5^{ij} points correspond to the creation or annihilation of a pair with one D_4^{+ij} and one D_4^{-ij} point.

6.1. *Evolutionary sequence of caustic mutations*

The dynamical evolution of a fluid goes along with a rich palet of local processes. These involve fundamental mutations in the local singularity structure that lead to significant topological changes of the spatial pattern forming in the fluid. In some systems and situations this will be a key element in the hierarchical buildup of structure. Another example where we can recognize such transformations is in the cascade of turbulent features down to ever smaller scales in the still largely ununderstood process of turbulence.

The fundamental notion in these structural mutations in the evolving fluid is that of the ruling dynamics of the system evoking changes in the deformation field. Small deformation will lead to the decay of singularities into different ones belonging to other singularity classes. Conversely, they may get folded according to a rigid order.

The sequence of singularity mutations is not random and arbitrary. Due to the strict geometric conditions and constraints corresponding to the various singularities, expressed in the caustic conditions discussed extensively in this study, a given singularity can allow transform into a restricted set of other singularities. Conversely, a given singularity may only have emanated from a restricted set of other singularities. In most situations a particular singularity can have decayed from only one distinctive class of singularities. Some may have descended from two other singularity classes. Likewise, most singularities can decay only into one distinctive other class of singularity. This is true for all A-family singularities. D-family singularities have a richer diversity of options, with the D_5 points being able to decay into 3 different ones, while the D_4 points may decay into 2 distinct A_3 points.

The entire singularity transformation and unfolding sequence may be transparently summarized in the unfolding diagram below.

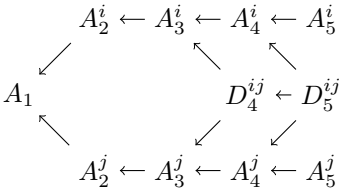

The unfolding diagram follows directly from Lagrangian catastrophe theory, although it can also be derived from the caustic conditions. The unfoldings of an A_k^i singularities into an A_{k-1}^i singularities, with $k \geqslant 2$, follow trivially from the caustic conditions. The same holds for the unfolding of the D_5^{ij} singularities into the D_4^{ij} singularities. The decau from the D_4 to the A_3 singularities are proven in section 4.2.1. The mutations $D_5^{ij} \to A_4^i$ and $D_5^{ij} \to A_4^j$ follow directly since the shell-crossing of the D_5^{ij} caustic is analogous to the shell-crossing condition on the A_4^i and A_4^j caustics.

7. Discussion

Caustics are important features in the dynamics of fluids, marking the positions where fluid elements cross and multi-stream regions form. These caustics can be associated to regions of infinite Lagrangian density and often indicate the formation of shocks. In large-scale structure formation, it can be shown that caustics indicate the regions in which non-linear gravitational collapse starts to take place and the cosmic web begins to form. In this setting, caustics can be used to build a skeleton of the caustic web, relating the non-linear gravitational collapse to the initial density fluctuations. For a 2-dimensional analysis of caustics of the cosmic web using the Zel'dovich approximation see Arnol'd *et al.* (1982); Hidding *et al.* (2014) and Feldbrugge *et al.* (2014). For a qualitative description of caustics in $(3+1)$-dimensional fluids see Arnol'd (1982).

This paper presents a novel proof of the caustic conditions in Lagrangian catastrophe theory. We discuss it extensively for the explicit situation of three-dimensional fluids, following up on those for one- and two-dimensional fluids. These were first derived by Arnol'd *et al.* (1982), for the specific situation of fluids with Hamiltonian dynamics. This was extended to general fluids by Bruce (1985). In their derivation they used concepts and methods from algebraic topology. In this paper, we argue and show that the classification of caustics can be completely understood in terms of geometric considerations. These

consist of shell-crossing conditions (equation (3.13)) in combination with elementary Morse theory Morse (1934); Milnor (1963).

Our derivation provides an alternative, more direct and transparent, route towards the classification of singularities as proposed by Arnol'd (Arnol'd 1976, 1982). It represents nothing less than an entirely new proof for the classification of Lagrangian catastrophes. Our scheme also allows us to extend these to general Lagrangian fluids in a space of arbitrary dimension. Its generic nature facilitates the derivation of generic caustic conditions, even for a fluid with arbitrary dynamics. The caustic conditions derived here, complement the qualitative description of 3-dimensional fluids presented in Arnol'd (1982).

In other words, we may even see the new formalism presented here as a reversal of the traditionally followed strategy. Traditionally, in the context of general catastrophe theory, the classification of Lagrangian caustics was proven using the classification of degenerate critical points. Here, we may have achieved the opposite: the geometric proof can be used to infer the classification of degenerate critical points, by shedding aside the reliance on concepts and methods of algebraic topology.

On the basis of the derived formalism, we subsequently show how the caustics of a Lagrangian fluid form an intricate skeleton of the non-linear evolution of the fluid. In Feldbrugge *et al.* (2017) we will study the application of the caustic conditions and the caustic skeleton to the three-dimensional cosmic web. The aim of this program is to improve our understanding of the formation of the cosmic web and attempt to analytically derive quantitative properties of the current large-scale structure.

Acknowledgements

We thank Sergei Shandarin for having raised our interest in caustics as a key towards the dynamical understanding of the cosmic web. We are grateful to Bernard Jones, Neil Turok and Gert Vegter for many useful and encouraging discussions. JF acknowledges the Perimeter Institute for facilitating this research through the support by the Government of Canada through the Department of Innovation, Science and Economic Development Canada and by the Province of Ontario through the Ministry of Research, Innovation and Science.

REFERENCES

Adler, R. J. 1981 *The Geometry of Random Fields*.

Aragón-Calvo, M. A., Platen, E., van de Weygaert, R. & Szalay, A. S. 2010*a* The Spine of the Cosmic Web. *Astrophys. J.* **723**, 364–382, arXiv: 0809.5104.

Aragón-Calvo, M. A., van de Weygaert, R. & Jones, B. J. T. 2010*b* Multiscale phenomenology of the cosmic web. *Mon. Not. R. Astron. Soc.* **408**, 2163–2187, arXiv: 1007.0742.

Arnol'd, V.I., Gusein-Zade, S.M. & Varchenko, A.N. 2012*a* *Singularities of Differentiable Maps, Volume 2: Monodromy and Asymptotics of Integrals*. Birkhauser Boston.

Arnol'd, V.I., Varchenko, A. & Gusein-Zade, S.M. 2012*b* *Singularities of Differentiable Maps: Volume I: The Classification of Critical Points Caustics and Wave Fronts*. Birkhauser Boston.

Arnol'd, V. I. 1972 Normal forms for functions near degenerate critical points, the Weyl groups of A_k, D_k, E_k and Lagrangian singularities. *Functional Anal. Appl* **6**, 1972.

Arnol'd, V. I. 1976 Wave front evolution and equivalent Morse lemma. *Communications in Pure Applied Mathematics* **29**, 557–582.

Arnol'd, V. I. 1978 *Mathematical methods of classical mechanics*.

Arnol'd, V. I. 1982 Evolution of singularities of potential flows in collisionless media

and transformations of caustics in three-dimensional space. *Trudy Seminar imeni G Petrovskogo* **8**, 21–57.

Arnol'd, V. I., Shandarin, S. F. & Zel'dovich, I. B. 1982 The large scale structure of the universe. I - General properties One- and two-dimensional models. *Geophysical and Astrophysical Fluid Dynamics* **20**, 111–130.

Bardeen, J. M., Bond, J. R., Kaiser, N. & Szalay, A. S. 1986 The statistics of peaks of Gaussian random fields. *The Astrophysical Journal* **304**, 15–61.

Bond, J. R., Kofman, L. & Pogosyan, D. 1996 How filaments of galaxies are woven into the cosmic web. *Nature* **380**, 603–606, arXiv: arXiv:astro-ph/9512141.

Bruce, J.W. 1985 A classification of 1-parameter families of map germs $r^3, 0 \to r^3, 0$ with applications to condensation problems. *J. Lond. Math. Soc.* **II. Ser. 30** (2), 375–384.

Cautun, M., van de Weygaert, R., Jones, B. J. T. & Frenk, C. S. 2014 Evolution of the cosmic web. *Mon. Not. R. Astron. Soc.* **441**, 2923–2973, arXiv: 1401.7866.

Creminelli, P., Nicolis, A., Senatore, L., Tegmark, M. & Zaldarriaga, M. 2006 Limits on non-Gaussianities from WMAP data. *Journal of Cosmology and Astroparticle Physics* **5**, 004, arXiv: astro-ph/0509029.

Delmarcelle, T. 1995 The Visualization of Second-Order Tensor Fields. PhD thesis, STANFORD UNIVERSITY.

Feldbrugge, Job 2014 Statistics of caustics in large-scale structure formation. Master's thesis, Rijksuniversiteit Groningen, the Netherlands.

Feldbrugge, J., Hidding, J. & van de Weygaert, R. 2014 Statistics of Caustics in Large-Scale Structure Formation. *Proceedings of IAU Symposium 308 "The Zeld'ovich Universe: Genesis and Growth of the Cosmic Web"* , arXiv: 1412.5121.

Feldbrugge, J., Hidding, J. & van de Weygaert, R. 2017 In preparation. *Mon. Not. R. Astron. Soc.* .

Goldstein, H. 1980 *Classical Mechanics*. Addison-Wesley.

Hidding, J., Shandarin, S. F. & van de Weygaert, R. 2014 The Zel'dovich approximation: key to understanding cosmic web complexity. *Mon. Not. R. Astron. Soc.* **437**, 3442–3472, arXiv: 1311.7134.

Komatsu, E., Kogut, A., Nolta, M. R., Bennett, C. L., Halpern, M., Hinshaw, G., Jarosik, N., Limon, M., Meyer, S. S., Page, L., Spergel, D. N., Tucker, G. S., Verde, L., Wollack, E. & Wright, E. L. 2003 First-Year Wilkinson Microwave Anisotropy Probe (WMAP) Observations: Tests of Gaussianity. *The Astrophysical Journal Supplement* **148**, 119–134, arXiv: astro-ph/0302223.

Landau, L.D. & Lifshitz, E.M. 1959 *Volume 1: Mechanics*. Pergamom.

Landau, L.D. & Lifshitz, E.M. 1976 *Volume 6: Fluid Mechanics*. Butterworth-Heinemann.

Milnor, J.W. 1963 *Morse Theory*. Princeton University Press.

Morse, M. 1934 *The calculus of variations in the large*. American Mathematical Society.

Planck Collaboration, Ade, P. A. R., Aghanim, N., Arnaud, M., Arroja, F., Ashdown, M., Aumont, J., Baccigalupi, C., Ballardini, M., Banday, A. J. & et al. 2016 Planck 2015 results. XVII. Constraints on primordial non-Gaussianity. *Astron. Astrophys.* **594**, A17, arXiv: 1502.01592.

Shandarin, S. F. & Zel'dovich, Y. B. 1989 The large-scale structure of the universe: Turbulence, intermittency, structures in a self-gravitating medium. *Reviews of Modern Physics* **61**, 185–220.

van de Weygaert, R. & Bond, J. R. 2008 Clusters and the Theory of the Cosmic Web. In *A Pan-Chromatic View of Clusters of Galaxies and the Large-Scale Structure* (ed. M. Plionis, O. López-Cruz & D. Hughes), *Lecture Notes in Physics, Berlin Springer Verlag*, vol. 740, p. 335.

Vasil'ev, V. A. 1978 Asymptotic exponential integrals, Newton's diagram, and the classification of minimal points. *Plenum Publishing Corporation* .

Zel'dovich, Y. B. 1970 Gravitational instability: An approximate theory for large density perturbations. *Astron. Astrophys.* **5**, 84–89.

Appendix A. Zel'dovich approximation

The Zel'dovich approximation is the first order approximation of a Lagrangian pressureless fluid evolving under self gravity, Zel'dovich (1970). The Zel'dovich approximation is the simplest example of a Lagrangian fluid with Hamiltonian dynamics and serves as a good illustration of the caustic conditions. The displacement map of the Zel'dovich approximation factors into a term depending on time and a term depending on the initial conditions

$$s(q,t) = -b_+(t)\nabla_q \Psi(q), \tag{A 1}$$

with the linearized velocity potential $\Psi(q)$ and growing mode $b_+(t)$. The growing mode can be obtained from linear Eulerian perturbation theory. Up to linear order, the linearized velocity potential is proportional to the linearly extrapolated gravitational potential at the current epoch $\phi_0(q)$, i.e.

$$\Psi(q) = \frac{2}{3\Omega_0 H_0^2}\phi_0(q), \tag{A 2}$$

with current Hubble constant H_0 and current energy density Ω_0. The linearized velocity potential $\Psi(q)$ encodes the initial conditions while the growing mode $b_+(t)$ encodes the cosmological evolution of the fluid. For the Zel'dovich approximation it is common to define the deformation tensor as

$$\psi_{ij} = \frac{\partial^2 \Psi(q)}{\partial q_i \partial q_j} \tag{A 3}$$

with eigenvalues $\lambda_i(q)$ satisfying $\mu_i(q,t) = -b_+(t)\lambda_i(q)$. The Lagrangian density in the Zel'dovich approximation can be expressed as

$$\rho(x',t) = \sum_{q\in A(x',t)} \frac{\rho_i(q)}{(1-b_+(t)\lambda_1(q))(1-b_+(t)\lambda_2(q))(1-b_+(t)\lambda_d(q))}, \tag{A 4}$$

with ρ_i the initial density field. Caustics occur at q at time t if and only if

$$\lambda_i(q) = \frac{1}{b_+(t)} \tag{A 5}$$

for at least one i. The eigenvalues λ_i are functions determined by the initial gravitational field. Equation A 5 can be pictured as a hyperplane at hight $1/b_+(t)$. The intersection of this plane with the graph of the eigenvalues undergoes shell-crossing at that time. For the Zel'dovich approximation the caustic conditions in terms of the eigenvalues λ_i are given by

$$A_1 = \{q \in L | \lambda_i(q) \neq 1/D_+(t) \text{ for all } t \text{ and } i\}, \tag{A 6}$$
$$A_2^i(t) = \{q \in L | \lambda_i(q) = 1/D_+(t)\}, \tag{A 7}$$
$$A_3^i(t) = \{q \in L | q \in A_2^i(t) \text{ and } \lambda_{i,i}(q) = 0\}, \tag{A 8}$$
$$A_4^i(t) = \{q \in L | q \in A_3^i(t) \text{ and } \lambda_{i,ii}(q) = 0\}, \tag{A 9}$$
$$A_5^i(t) = \{q \in L | q \in A_4^i(t) \text{ and } \lambda_{i,iii}(q) = 0\}, \tag{A 10}$$
$$D_4^{\pm ij}(t) = \{q \in L | \lambda_i(q) = \lambda_j(q) = 1/D_+(t) \text{ and } \mathrm{sign}(S_{\mathcal{M}}) = \pm 1\}, \tag{A 11}$$
$$D_5^{ij}(t) = \{q \in L | q \in D_4^{ij}(t) \text{ and } (\lambda_i - \lambda_j)_{,i}(q) = (\lambda_i - \lambda_j)_{,j}(q) = 0\}, \tag{A 12}$$

and the points at which the topology of above sets changes

$$A_3^{i+} = \{q \in L | q \in A_2^i \wedge \lambda_i(q) \text{ max-/minimum of } \lambda_i\}, \tag{A 13}$$
$$A_3^{i-} = \{q \in L | q \in A_2^i \text{ saddle point of } \lambda_i\}, \tag{A 14}$$

$$A_4^{i+} = \{q \in L | q \in A_3^i \wedge \lambda_{i,ii}(q) \text{ max-/minimum of } \lambda_{i,ii}|_{A_2}\}, \tag{A 15}$$

$$A_4^{i-} = \{q \in L | q \in A_3^i \text{ saddle point of } \lambda_{i,ii}|_{A_2}\}, \tag{A 16}$$

$$D_4^{ij\pm} = \{q \in L | q \in D_4^{\pm ij} \wedge \lambda_i(q) = \lambda_j(q) \text{ max-/minimum of } \lambda_i|_{D_4^{\pm ij}} = \lambda_j|_{D_4^{\pm ij}}\} \tag{A 17}$$

with the direction derivatives $\lambda_{i,i} = \nabla\lambda_i \cdot v_i, \lambda_{i,ii} = \nabla\lambda_{i,i} \cdot v_i$ and $\lambda_{i,iii} = \nabla\lambda_{i,ii} \cdot v_i$. Note that the eigenvectors are defined modulo multiplication by a real number and really represent lines.

Appendix B. Lagrangian maps and Lagrangian equivalence

We here shortly describe the mathematical background of symplectic manifolds, Lagrangian manifolds and Lagrangian maps. For a detailed description and derivations we refer to Arnol'd *et al.* (2012*a*,*b*).

B.1. *Symplectic manifolds and Lagrangian maps*

A $2n$-dimensional symplectic manifold (M, ω) is a smooth $2n$-dimensional manifold M, equipped with a closed nondegenerate bilinear 2-form ω called the symplectic form. Symplectic manifolds are always even dimensional for ω to be nondegenerate. In Hamiltonian dynamics the symplectic form ω can be associated to the Poisson brackets which encodes the dynamics of the theory. A Lagrangian manifold L of a $2n$-dimensional symplectic manifold (M, ω) is a n-dimensional submanifold of M on which the symplectic form ω vanishes. Let (B, π) be a Lagrangian fibration of (M, ω), which is a n-dimensional manifold with a projection map $\pi : M \to B$ for which the fibers $\pi^{-1}(b)$ are Lagrangian manifolds for all $b \in B$.

An example of a symplectic manifold is phase space consisting of position and canonical momenta $(q_1, \dots, q_n, p_1, \dots p_n)$ with the symplectic form $\omega = \sum_i^n \mathrm{d}q_i \wedge \mathrm{d}p_i$. An example of a Lagrangian fibration is $\{(q_1, \dots, q_n), \pi\}$ with the projection map $\pi(q_1, \dots, q_n, p_1, \dots p_n) = (q_1, \dots, q_n)$.

Give a symplectic manifold (M, ω) with a Lagrangian fibration (B, π) we can for every Lagrangian manifold L define a Lagrangian map $(\pi \circ i) : L \to M \to B$, with i being the inclusion map sending L into M. Two Lagrangian maps $(\pi_1 \circ i_1) : L_1 \to M_1 \to B_1$ and $(\pi_2 \circ i_2) : L_2 \to M_2 \to B_2$ are defined to be Lagrangian equivalent if there exist diffeomorphisms σ, τ and ν such that $\tau \circ i_1 = i_2 \circ \sigma, \nu \circ \pi_1 = \pi_2 \circ \tau$ and $\tau^* \omega_2 = \omega_1$, or equivalently the diagram below commutes

$$\begin{array}{ccccc} L_1 & \xrightarrow{i_1} & (M_1, \omega_1) & \xrightarrow{\pi_1} & B_1 \\ \sigma\downarrow & & \tau\downarrow & & \nu\downarrow \\ L_2 & \xrightarrow{i_2} & (M_2, \omega_2) & \xrightarrow{\pi_2} & B_2 \end{array}$$

B.2. *Displacement as Lagrangian map*

Given a Lagrangian submanifold $\mathcal{L}$ we can construct a corresponding Lagrangian map. First map the Lagrangian submanifold $\mathcal{L}$ with the inclusion map $i : \mathcal{L} \to \mathcal{C}$ to the corresponding points in phase space $\mathcal{C}$, i.e., $i : (q, x) \mapsto (q, x)$ for all $(q, x) \in \mathcal{L}$. Subsequently map these points to a base manifold B with the projection map $\pi : \mathcal{C} \to B$. In Lagrangian fluid dynamics it is convenient to pick the Eulerian manifold E as the base manifold B and define the projection map as $\pi : (q, x) \mapsto x$ for all $(q, x) \in \mathcal{C}$. As there will always be an exact correspondence between the Lagrangian manifold L and the Lagrangian submanifold $\mathcal{L}_t \subset \mathcal{C}$ (there exists a unique point $x \in E$ such that

$A_1:\ x(q,1)=(q_1,q_2,q_3)$	$1+\mu_1=1$	$1+\mu_2=1$	$1+\mu_3=1$
$A_2:\ x(q,1)=(q_1,q_2,q_3^2)$	$1+\mu_1=1$	$1+\mu_2=1$	$1+\mu_3=2q_3$ $\mu_{3,3}=2$
$A_3:\ x(q,1)=(q_1,q_2,q_1q_3+q_3^3)$	$1+\mu_1=1$	$1+\mu_2=1$	$1+\mu_3=3q_3^2+q_1$ $\mu_{3,3}=6q_3$ $\mu_{3,333}=6$
$A_4:\ x(q,1)=(q_1,q_2,q_1q_3+q_3^4)$	$1+\mu_1=1$	$1+\mu_2=1$	$1+\mu_3=q_1+4q_3^3$ $\mu_{3,3}=12q_3^2$ $\mu_{3,33}=24q_3$ $\mu_{3,333}=24$
$A_5:\ x(q,1)=(q_1,q_2,q_1q_3+q_2q_3^2+q_3^5)$	$1+\mu_1=1$	$1+\mu_2=1$	$1+\mu_3=q_1+2q_2q_3+5q_3^4$ $\mu_{3,3}=2q_2+20q_3^3$ $\mu_{3,33}=60q_3^2$ $\mu_{3,333}=120q_3$ $\mu_{3,3333}=120$
$A_3^{\pm}:\ x(q,1)=(q_1,q_2,(q_1^2\pm q_2^2)q_3+q_3^3)$	$1+\mu_1=1$	$1+\mu_2=1$	$1+\mu_3=q_1^2\pm q_2^2+3q_3^2$ $\mu_{3,3}=6q_3$ $\mu_{3,33}=6$
$A_4^{\pm}:\ x(q,1)=(q_1,q_2,q_1q_3\pm q_2^2q_3^2+q_3^4)$	$1+\mu_1=1$	$1+\mu_2=1$	$1+\mu_3=q_1\pm 2q_2^2q_3+4q_3^3$ $\mu_{3,3}=\pm 2q_2^2+12q_3^2$ $\mu_{3,33}=24q_3$ $\mu_{3,333}=24$

Table 1: The caustic conditions of the normal forms of the A singularity classes

$(q,x)\in\mathcal{L}_t$ for every $q\in L$), we can associate the Lagrangian map corresponding to $\mathcal{L}_t$ with the map x_t. In summary, the map x_t corresponds uniquely to a Lagrangian map for fluids with Hamiltonian dynamics.

A Lagrangian map can develop regions in which multiple points in the Lagrangian manifold are mapped to the same point in the base space. The points at which the number of pre-images of the Lagrangian map changes are known as Lagrangian singularities. Lagrangian catastrophe theory classifies the stable singularities, stable with respect to small deformations of $\mathcal{L}$, up to Lagrangian equivalence. Lagrangian equivalence is a generalization of equivalence up to coordinate transformations. For a precise definition of Lagrangian equivalence we refer to appendix B.

B.3. *Lagrangian map germs*

In catastrophe theory it is important to consider the Lagrangian map at a point. This is achieved by means of Lagrangian germs. Starting with a point $p\in M$ we can consider Lagrangian functions $F_i: U_i\to B$ for $i=1,2$ for small environments U_i of p which coincide on the intersection $U_1\cup U_2$. The equivalence classes of such Lagrangian functions are Lagrangian germs. The Lagrange equivalence of Lagrangian maps straightforwardly extends to Lagrange equivalence of Lagrangian germs. These are the equivalence classes used in the classification of stable Lagrangian maps, where a Lagrangian germ is stable if and only if every sufficiently small fluctuation on the germ is Lagrange equivalent to the germ.

B.4. *Gradient maps*

Every Lagrangian germ is Lagrange equivalent to the germ of a gradient map. That is to say, for every Lagrangian map $l = \pi \circ i : \mathcal{L} \to \mathcal{C} \to E$ we can for a point $(q, x) \in \mathcal{L}$ locally write the map as

$$l(q_1, \ldots, q_n, x_1, \ldots, x_n) = \left(\frac{\partial S}{\partial q_1}, \frac{\partial S}{\partial q_2}, \ldots, \frac{\partial S}{\partial q_n} \right) \tag{B 1}$$

for some function $S : \mathbb{R}^n \to \mathbb{R}$. The corresponding map x is given by

$$x(q_1, \ldots, q_n, t) = \left(\frac{\partial S}{\partial q_1}, \frac{\partial S}{\partial q_2}, \ldots, \frac{\partial S}{\partial q_n} \right) \tag{B 2}$$

for some time t. By writing $S = \frac{1}{2}q^2 + \Psi$ for $\Psi : \mathbb{R}^3 \times \mathbb{R} \to \mathbb{R}$ we obtain

$$x(q, t) = q + \frac{\partial \Psi}{\partial q}, \tag{B 3}$$

with the gradient field

$$s = \frac{\partial \Psi}{\partial q}. \tag{B 4}$$

The Jacobian of the displacement map

$$\left[\frac{\partial s}{\partial q} \right]_{ij} = \frac{\partial^2 \Psi}{\partial q_i \partial q_j} \tag{B 5}$$

is symmetric. The set of eigenvectors $\{v_i\}$ can be taken to be orthonormal by which the dual vectors coincide with the eigenvectors, i.e., $v_i^* = v_i$ for all i. A Lagrangian map is locally equivalent to the Zel'dovich approximation.

B.5. *Arnol'ds Classification of Lagrangian catastrophes*

In section 4.1, we described the classification of Lagrangian singularities in up to three dimensions. However the classification extends to higher dimensional singularities. A $(n+1)$-dimensional fluid can contain stable singularities in the A_i, D_i and E_i classes with $i \leqslant n+2$, where the D-class range starts at $i = 4$ and the E-class is only defined for $i = 6, 7, 8$. These singularities decompose into lower-dimensional singularities as illustrated in the unfolding diagram below.

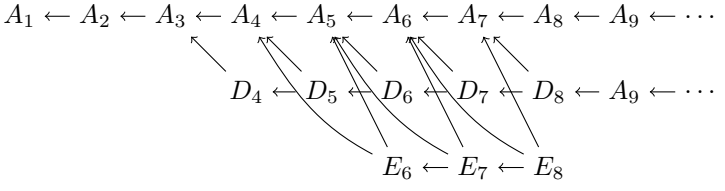
$A_1 \leftarrow A_2 \leftarrow A_3 \leftarrow A_4 \leftarrow A_5 \leftarrow A_6 \leftarrow A_7 \leftarrow A_8 \leftarrow A_9 \leftarrow \cdots$
$D_4 \leftarrow D_5 \leftarrow D_6 \leftarrow D_7 \leftarrow D_8 \leftarrow A_9 \leftarrow \cdots$
$E_6 \leftarrow E_7 \leftarrow E_8$

Appendix C. Caustic conditions of the normal forms

We here verify the caustic conditions for the normal forms in the generic classification of singularities given in section 5.3. The normal forms of the the Lagrangian singularities given in section 5.4 follow analogously.

The eigenvalue fields and corresponding derivatives in the direction of the eigenvector fields are given in table 1. The eigenvalues of the normal form for the trivial (A_1) case equal 1 and thus satisfy the condition $1 + \mu_i \neq 0$ for all i. The third eigenvalue of the normal form of the fold (A_2) singularity equals -1 in the origin. The derivative of the eigenvalue field in the direction of the corresponding eigenvector field does not vanish in the origin. The normal form thus satisfies the caustic conditions of the fold singularity. The normal forms of the remaining singularities follow analogously.